# Space Programs Summary No. 37-31, Volume VI

for the period November 1, 1964 to December 31, 1964

## Space Exploration Programs and Space Sciences



GPO PRICE $ _____

OTS PRICE(S) $ _____

Hard copy (HC) 3.00

Microfiche (MF) .50

JET PROPULSION LABORATORY
CALIFORNIA INSTITUTE OF TECHNOLOGY
PASADENA, CALIFORNIA

January 31, 1965

# *Space Programs Summary No. 37-31, Volume VI*

*for the period November 1, 1964 to December 31, 1964*

## *Space Exploration Programs and Space Sciences*

JET PROPULSION LABORATORY
CALIFORNIA INSTITUTE OF TECHNOLOGY
PASADENA, CALIFORNIA

January 31, 1965

# Preface

The *Space Programs Summary* is a six volume, bimonthly publication designed to report on JPL space exploration programs, and related supporting research and advanced development projects. The subtitles of all volumes of the *Space Programs Summary* are:

Vol. I. The Lunar Program (Confidential)

Vol. II. The Planetary–Interplanetary Program (Confidential)

Vol. III. The Deep Space Network (Unclassified)

Vol. IV. Supporting Research and Advanced Development (Unclassified)

Vol. V. Supporting Research and Advanced Development (Confidential)

Vol. VI. Space Exploration Programs and Space Sciences (Unclassified)

The *Space Programs Summary,* Volume VI consists of an unclassified digest of appropriate material from Volumes I, II, and III; an original presentation of the JPL (1) quality assurance and reliability efforts, and (2) environmental- and dynamic-testing facility-development activities; and a reprint of the space science instrumentation studies of Volumes I and II. This instrumentation work is conducted by the JPL Space Sciences Division and also by individuals of various colleges, universities, and other organizations. All such projects are supported by the Laboratory and are concerned with the development of instruments for use in the NASA space flight programs.

W. H. Pickering, *Director*
*Jet Propulsion Laboratory*

**Space Programs Summary No. 37-31, Volume VI**



Prepared under Contract No. NAS 7-100, National Aeronautics & Space Administration

# Contents

## LUNAR PROGRAM



## PLANETARY–INTERPLANETARY PROGRAM



## DEEP SPACE NETWORK



## SUPPORTING ACTIVITIES

# Contents (Cont'd)

## SPACE SCIENCES

LUNAR PROGRAM

# I. *Ranger* Project

## A. Introduction

The *Ranger* Project was established to develop a space flight technology for transporting engineering and scientific instruments to the Moon and planets. Of the nine *Ranger* launchings, using *Atlas D–Agena B* vehicles, now planned, seven flights have been made.

*Rangers I* and *II* (Block I) were not lunar-oriented, but were engineering evaluation flights to test the basic systems to be employed in later lunar and planetary missions. Several scientific experiments were carried on a non-interference basis. Both spacecraft performed satisfactorily within the constraints of the obtained satellite orbit. *Rangers III*, *IV*, and *V* (Block II) carried a gamma-ray instrument, a TV camera, and a rough-landing seismometer capsule; each of these flights experienced failures.

The objective of the *Ranger* Block III (*Rangers VI, VII, C,* and *D*)[1] flights is to obtain pictures of the lunar surface, at least an order of magnitude better than those obtainable with Earth-based photography, which will be of benefit to both the scientific program and the U.S. manned lunar flight program. The *Ranger VI* spacecraft, which was launched from the Air Force Eastern Test Range on January 30, 1964, and impacted the Moon essentially on target on February 2, 1964, did not accomplish the primary flight objective due to a failure of the TV subsystem to transmit pictures. An extensive analysis of the TV subsystem failure was conducted, new and reworked hardware was assembled as the *Ranger VII* TV subsystem, and extensive testing of the reassembled TV subsystem was performed. The *Ranger VII* spacecraft was launched from the Air Force Eastern Test Range on July 28, 1964, and impacted the Moon on target on July 31, 1964. The mission flight objective was accomplished. The outstanding events of the mission were the precision of the trajectory correction and the transmission of 4304 video pictures of the lunar surface.

The updating operations and scheduled tests for the *Ranger* proof test model (PTM) were completed. The PTM will be maintained in the *Ranger C* and *D* configuration for use in evaluating any problems that might develop during these missions. *Rangers C* and *D* are in various stages of assembly; subsystem and system tests are being performed.

[1]*Rangers C* and *D* are the two spacecraft presently designated to complete the *Ranger* Block III Project.

# B. Spacecraft Systems Testing

## 1. Ranger C

System Test 3 was conducted at JPL on October 26, 1964. The spacecraft was exposed to both on-board and off-board RF sources. The "usual" interference was noted on the data encoder Address 90 measurements, but was not considered a problem.

Preparation for the explosive safe area (ESA) simulation tests, begun October 27, included an operational test of the flight secondary Sun sensors located on the solar panels. All checks indicated proper operation. The midcourse propulsion subsystem was also installed in the spacecraft with live pyrotechnics on that date.

Tests and operations from October 28 to November 9 were as follows: TV full-power RF test; Lockheed Missiles and Space Company (LMSC) adapter and shroud arrival and inspection; electrical checks on adapter wiring; determination of preload values for mating of spacecraft feet to LMSC adapter; matchmate of spacecraft to LMSC adapter; shroud omni-antenna coupler adjustment; RF transmission loss measurements; TV shroud light compatibility checks; operational checkout of spacecraft at ESA (simulated); precountdown and countdown dummy runs; pyrotechnic subsystem verification (RF link with electromagnetic interference); attitude-control and midcourse propulsion pressure transducer calibration with data encoder; replacement of attitude-control derived-rate module with flight unit and partial subsystem test; rework of TV subsystem to ensure flight status prior to environmental tests; and final checks and remate of the TV subsystem on the spacecraft bus.

Following the reassembly of the TV subsystem, an evaluation of camera operation indicated unacceptable performance from Camera P4. To allow time for further evaluation, the TV subsystem was assembled to the bus, and weight and center-of-gravity measurements were performed. The following day, the TV subsystem problem investigation was resumed. After several tests, a miswired ground on Camera P4 was corrected, and a shutter on Camera P2 was replaced. A replacement Camera P4 and associated electronics were installed and checked out November 12.

Vibration testing of the spacecraft was conducted November 16 to 20. This testing included the following operations: modal verification, $x$-axis noise vibration; $x$-axis low- and high-frequency vibration; the complete $y$-axis vibration series (performed with no direct-access cabling attached to the spacecraft); torsional vibration; adjustment of attitude-control pressure vessel Belleville springs to flight value; preparation for $z$-axis vibration, including blast mat installation and pressurization of the attitude-control gas subsystems to approximately flight pressures; $z$-axis vibration; depressurization of the gas subsystems; and post-vibration modal verification.

No problems were encountered during the antenna deflection test and post-vibration system test which followed. During the pre-mission test verification, a problem was encountered in transferring the spacecraft power from "external" to "internal." Investigation revealed an out-of-tolerance switch in the power switch and logic module, necessitating replacement of the module.

The midcourse sequence of Mission Test 1 at high temperatures was conducted December 2, and the terminal sequence December 4. Two problems occurred during the test: (1) The TV subsystem backup clock was out of the allowable 5-min tolerance, and telemetry pulses indicated that the clock was unstable; and (2) the resolution of Camera P4 was out-of-tolerance.

Mission Test 2 at low temperatures was begun December 4. In order to determine the magnitude of the Camera P4 resolution problem, a special TV subsystem turn-on test was run prior to the midcourse sequence. This test was performed with the TV subsystem temperature at 25°C, the highest expected in flight, to determine the resolution of Camera P4 at this temperature. The resolution improved to within specification value, and the decision was made to continue the test and not replace or refocus the camera. The midcourse sequence was completed on December 5, and cruise-mode conditions were re-established the following day. The terminal sequence of Mission Test 2 will be discussed in the next issue of the *Space Programs Summary*, Vol. VI.

## 2. Ranger D

The mechanical assembly operations completed November 13 included a satisfactory quantitative leak check on the attitude-control gas subsystem in the Spacecraft Assembly Facility pit. Ground wiring and electrical integrity checks and initial power application were successfully performed. All subsystem tests and calibrations with telemetry were completed by November 30, except for the pressure transducer calibrations and the TV subsystem test. The significant problems during the checks,

now under study, were an open fuse in a data encoder module and excessive noise on the communications ground receiver phase error.

The TV subsystem arrived at the Spacecraft Assembly Facility on December 4. Post-shipment verification tests and camera gain checks indicated that all camera gains were 15 to 25% high and would require readjustment prior to mating of the TV subsystem to the spacecraft bus.

A system test was performed on December 4 without the TV subsystem. The only significant anomaly in this test was a B2-1 event noted on the telemetry while motion checks on the spacecraft were being performed. The event apparently was the result of a gyro capacitor charge event by the central computer and sequencer (CC&S). This condition was found to be coincident with the system test fixture motor-start transient, which somehow was coupled into the CC&S.

A power survey on December 5 revealed a noise level higher than specification on the Command Converter 4A5 6-v dc output. The unit was replaced with a spare 4A5, and the noise level was then within specification.

## C. Thermal Characteristics of *Ranger* C TV Subsystem

From September 19 to October 7, four series of thermal-vacuum tests were performed on the *Ranger C* TV subsystem at RCA. Actually, the tests were electrical verification tests in which the terminal-mode operations of the TV subsystem were exercised in a simulated space environment, with each test run starting from a predetermined average cruise-mode temperature. A thermal-balance test was not required since the TV subsystem had been thermally tested prior to electrical modification. These previous tests showed that the *Ranger C* TV subsystem had thermal characteristics similar to those of the *Ranger VII* TV subsystem. The temperature data obtained during the thermal-vacuum tests were normal.

The thermal finishes employed on the TV subsystem during the *Ranger VII* mission provided desirable cruise-mode temperatures to all portions of the TV subsystem. There is no reason to change the average temperature of the over-all spacecraft or to alter the thermal distribution within the TV subsystem for the *Ranger C* mission. One exception to this is the application of a white paint to the antenna ring, resulting in a slightly lower temperature in the cameras.

Terminal-mode temperatures of the *Ranger C* TV subsystem will be affected to a limited degree by changes in equipment from the *Ranger VII* design. The only equipment changes made thus far are in the intermediate power amplifiers of the transmitter assemblies and in the battery mounting bars. The configuration of intermediate power amplifiers incorporating the Resdel cavity was found to operate considerably cooler than the configuration used in the *Ranger VII* TV subsystem. The change in construction material of the battery support bars will have little or no effect on battery temperatures.

During the final hours of the *Ranger VII* flight, a temperature increase of 7 or 8°F was noted in the camera-lens-housing telemetry. It has been found that the flux density of thermal energy as the spacecraft approaches the lunar surface is sufficient to cause the encountered temperature increase. The *Ranger C* spacecraft can be expected to encounter a rise in temperature of 7.5 to 8.5°F in the area of the camera lens housing during the last 3 hr of flight.

# II. *Surveyor* Project

## A. Introduction

The *Surveyor* Project will take the next step in developing lunar technology by attempting soft landings on the Moon with a group of test missions whose objective is to demonstrate successful soft landing by post-landing spacecraft operation. An engineering payload including elements of redundancy, increased diagnostic telemetry, touchdown instrumentation, and survey TV will be used.

Following the test missions, the general objective is to conduct lunar exploration to extend our knowledge of the nature of the Moon and to discover and verify the suitability of sites for *Apollo* spacecraft landings. These flights will carry a scientific payload selected from the following experiments: two-camera TV, micrometeorite ejecta, single-axis seismometer, alpha-particle scattering, soil properties (surface sampler), and touchdown dynamics.

Through 1966, spacecraft will be injected into the lunar trajectory by direct ascent, using single-burn *Atlas–Centaur* vehicles. For launches prior to 1966, a 50-m/sec midcourse correction capability will exist. Launches performed in 1966 will require a 30-m/sec midcourse correction capability.

Hughes Aircraft Company (HAC) is under contract to develop and manufacture the first seven spacecraft.

## B. Systems

### 1. SC-1 Flight-Acceptance Testing

Group tests on the SC-1 flight spacecraft power subsystem were completed by HAC. Then, using the spacecraft power subsystem, the remaining group tests [except those of the radar altimeter and doppler velocity sensor (RADVS)] were performed. Because of the lack of spacecraft units, the flight-control, altitude-marking-radar, and signal-processing group tests could not be performed prior to the start of the upgrading modification period.

Improvements to correct these problems will be incorporated during the upgrade period. The spacecraft harness will be thermally wrapped in preparation for the solar-thermal-vacuum (STV) testing to be performed on completion of the system functional test phase.

### 2. T-21 Prototype Vehicle Testing

A complete RADVS group test was performed on the QA-1 system installed on the T-21 vehicle at HAC. Although the data indicated a few out-of-tolerance conditions, the over-all system operation was considered satisfactory for continued testing.

The STV test equipment was checked out using the M-12 spacecraft mockup and was then installed in the actual T-21 STV vehicle.

Chamber emergency-shutdown modifications were completed and functionally tested. The operations techniques and modifications to the chamber demonstrate that the system is able to satisfactorily accomplish a shutdown in the event of total power failure.

### 3. T-2 Simplified Spacecraft Closed-Loop Testing

The T-2 closed-loop test program was designed to evaluate the flight-control electronics in a simulated dynamic condition such as that in the planned T-2 drop missions. The tests were conducted at the Air Force Missile Development Center (AFMDC), where the T-2 vehicle, cables, test equipment, and hardware could be used in flight configuration. The T-21 system test equipment assembly (STEA) was modified for use as closed-loop simulation equipment.

The tests were performed as a mixed simulation in which the closed-loop equipment was utilized to simulate the electrical analog of the T-2 vehicle geometry and dynamics, vehicle mass, aerodynamic drag, and engine thrust. These tests differed from previous closed-loop tests in that the lateral velocity, acceleration, and trajectory control loops were included in the simulation. The gyros and accelerometer were electrically torqued. The RADVS was alternately replaced by the electrical transfer function and was incorporated in the system such that only the microwave operation was simulated by the STEA. Velocity and rate loops were closed and examined for stability and performance in simulated mission profiles. Acoustic and radar noise were introduced to evaluate system performance.

The T-2 closed-loop test program verified that the T-2 vehicle flight-control hardware performs in accordance with design requirements and mission objectives. The equipment is stable under simulated system operation. The system parameters which were measured were found to correspond to the results of the analog computer and design analysis studies which define the T-2 flight-control system. The integration of the RADVS with the flight-control electronics resulted in a compatible system in closed-loop operation. Injection of acoustic and electronic radar noise at system operation levels resulted in performance which is acceptable for mission success.

### 4. T-2 Drop Testing

During a recent T-2 drop test, operation of the pitch and yaw inertial hold control loops was satisfactory. At touchdown, the telemetered pitch and yaw gyro angles were within 1 deg of the vehicle angles at which the inertial hold mode was initiated. At vernier-engine ignition, the vehicle started a slow rolling motion which continued until impact. It was found that a failure in the roll gyro AC amplifier prevented the roll control system from operating properly. Investigation of the AC amplifier malfunction disclosed that the output transistors had failed, apparently from excessively high surge currents. A review of the circuit design indicated that component safety margins were adequate. The cause of the excessive current is still under investigation.

### 5. S-8/RADVS Vibration Testing

This test was conducted to demonstrate satisfactory operation of the RADVS system on a flight-type spaceframe when subjected to the vibrational environment expected to result from firing the vernier engines. The presence of any radar interference attributable to vibratory excitation of the footpads or crushable blocks was explored. Data were taken to establish adequate functional performance criteria for individual antennas when subjected to random vibration.

To meet the test objectives, it was necessary to operate the RADVS system with no interference from surrounding objects. This was accomplished by mounting the S-8 vehicle in an inverted position on a shock cord suspension system, with vibration exciters coupled to vernier-engine dummies (Fig. 1). The vehicle was mounted with legs extended and crushable blocks installed. Three vibration exciters, a power amplifier system, and a random console system were used. Drive link assemblies attached

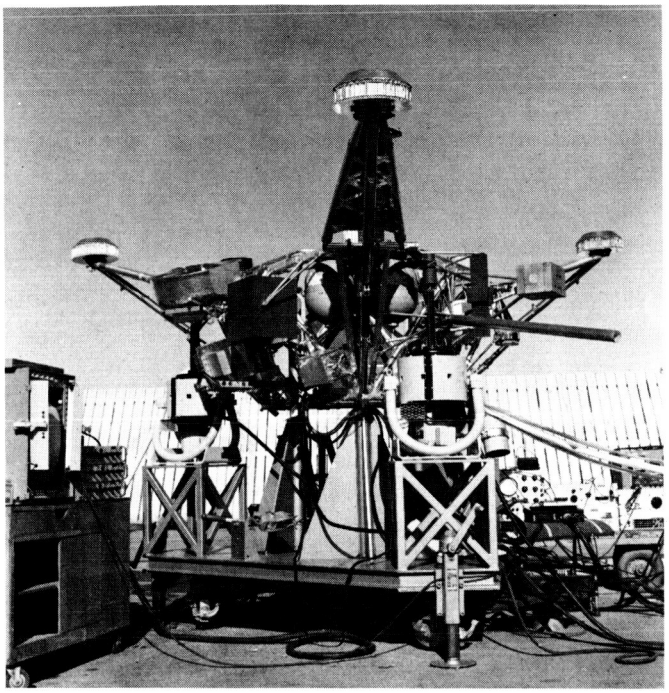

**Fig. 1. S-8 vehicle inverted on test fixture**

the vibration exciters to the vehicle. Piezoelectric-type force gages were installed between the drive links and the vernier-engine dummies. The S-8 vehicle configuration represented the spacecraft just after retro-engine ejection and during vernier-engine operation. In general, the results to date seem to indicate that the excitation method using three vibration exciters driven from a single power amplifier has proven to be quite satisfactory.

Preceding the vibration tests, an abbreviated RADVS group quantitative checkout was conducted. At the completion of a vibration phase, the vehicle was returned to the hangar for a post-test checkout and reinstallation of the succeeding RADVS system.

On-line RADVS testing consisted basically of monitoring the RADVS signals. The data obtained indicated the presence of preamplifier residual noise. Therefore, preamplifier outputs which locked up could be observed during the various phases of vibration testing. Since this was the first time the RADVS system was vibrated in a spacecraft while operating with no interference from surrounding objects, additional tests were conducted with antenna dummy loads installed. Results of these tests provided calibration for the RADVS for future vibration tests when dummy loads may be required.

From the results of T-2 firings at the AFMDC, the engine accelerometer level was found to be on the order of 1.8-*g* rms. Engine responses for the S-8/RADVS vibration tests at HAC measured as high as 10.5-*g* rms, indicating a rather large margin of satisfactory RADVS operation.

# C. Engineering Mechanics

## 1. Ground Clearance During Touchdown

A minimum ground clearance of 4.2 in. (to the bottom of the square tube) for a 20-ft/sec vertical velocity and an estimated minimum ground clearance of 5 to 5½ in. for a 15-ft/sec vertical velocity have been established as criteria for the present A-21 *Surveyor* spacecraft based on a $3\sigma$ flight-control dispersion ellipse relating lateral velocity and incidence at touchdown. The practicability of improving *Surveyor* ground clearance during touchdown was evaluated by HAC. The investigation was made on the basis of simple changes to the landing gear geometry. The corresponding effect of these changes on stability and loads was also assessed or estimated.

The simplest changes that can be made to the landing gear design to improve ground clearance are: (1) increase in foot height, (2) increase in leg length, and (3) increase in leg inclination to the vehicle $x$-$y$ plane. The changes could be incorporated into the vehicle singly or in any of several combinations if the envelope limitations with respect to the *Centaur* shroud were not violated.

It appears that increases in ground clearance can be best achieved by increases in leg inclination and foot height, since increase of these quantities by the amounts considered does not deteriorate stability when no corresponding increase is made in crushable block height. When the crushable blocks are lengthened, however, it may be necessary to lengthen the legs to maintain acceptable stability characteristics. Increase in the length-to-diameter ratio of the blocks may be a problem due to side loads. Load levels would be expected to increase 15% for the leg inclination change, but should not be appreciably affected by an increase in foot height.

The investigation indicated that a 3½-in. increase in foot height with an appropriate increase in block height

should yield a clearance increase of about 2 in. with no load or stability penalties. A more detailed analysis of the possibility of increasing clearance by increasing leg inclination is required. Changes in footpad and crushable block size or position must be evaluated carefully with respect to rocket exhaust heating and changes in radar performance.

### 2. T-2SS Spaceframe and Parachute Attachment

Extensive redesign has been incorporated in the T-2SS vehicle (backup vehicle for T-2 drop tests) spaceframe and parachute harness as a result of changes in the parachute deployment mechanism and a need for weight reduction. Since the early drop tests of the T-2 vehicle, including actual parachute deployments, the vehicle weight has increased from 165 to approximately 210 lb. Therefore, structural verification tests of the upper main spaceframe cluster and parachute attachment were performed for the increased load magnitude.

Loads were applied to the test specimen in three directions (Fig. 2). The test specimen was rigidly attached at the base to the laboratory structure, and impact loads were applied to the end of the parachute cord. The desired rate of loading during the tests was obtained experimentally by adjusting the drop weight and height

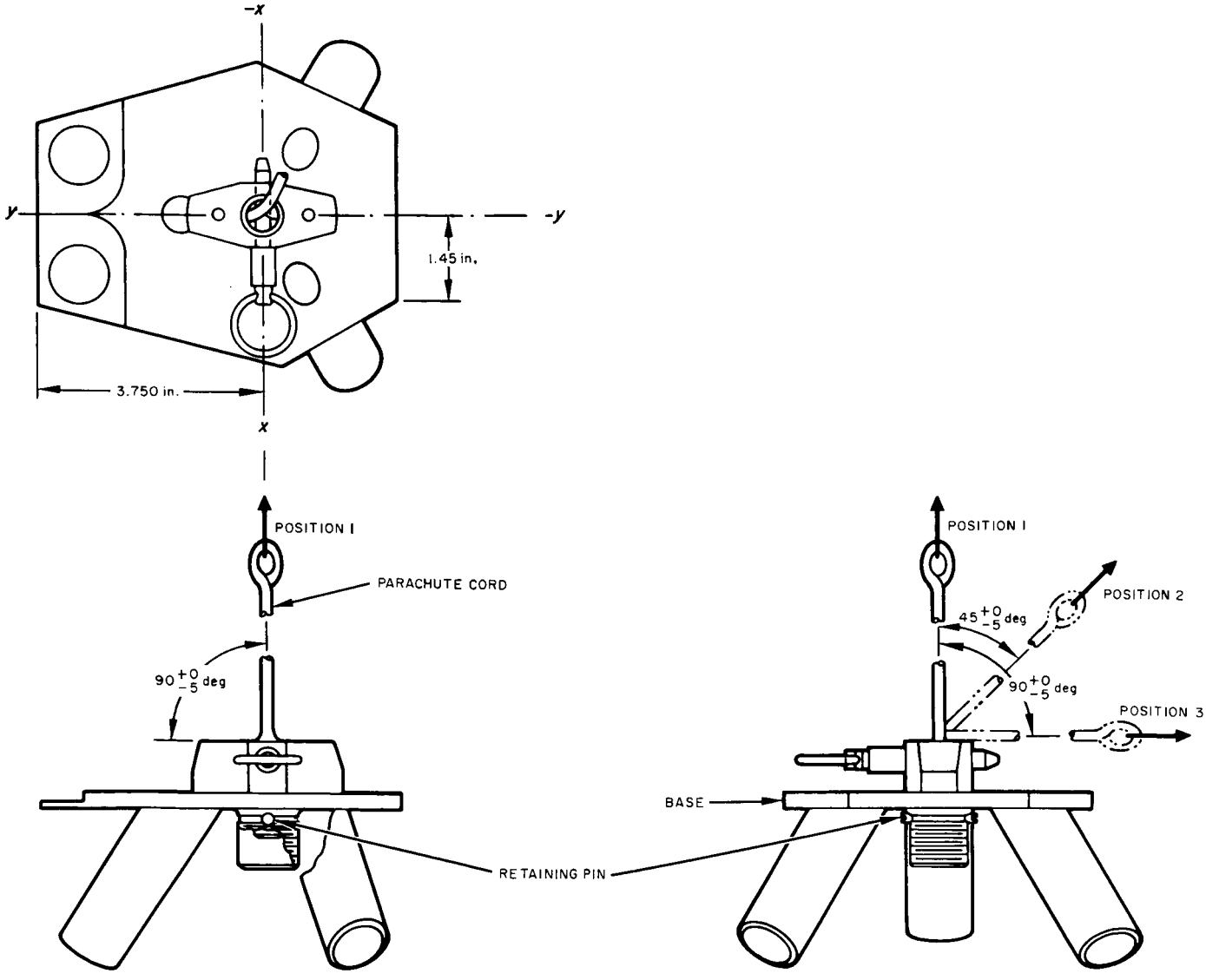


**Fig. 2. T-2SS spaceframe and parachute attachment test setup**

and by monitoring the load cell mounted in series. The rate of loading used was based on accelerometer data obtained during actual parachute deployment drop tests of the T-2 vehicle. The design requirement was the application of 2000-lb peak load as a half sine wave in 0.10 sec, which corresponds to an acceleration of approximately 9 $g$ (ultimate) acting on the vehicle at the time of parachute deployment.

All metal parts were inspected for permanent damage following each test phase and were found to be satisfactory. The parachute cords became frayed, and four cords failed during the repeated load tests. A cord with a rating of 3000 lb was used to complete the impact tests. However, since the peak load used is the maximum (ultimate) load predicted for the spaceframe and is far too severe for the actual cord, no design change was made. Additional repetitive static-load tests at limit load are currently being performed by HAC to ascertain if fraying and breakage of the parachute cord under repeated loading could be a problem.

### 3. Antenna Solar Panel Positioner

The antenna solar panel positioner provides mounting, positioning, position indicators, and launch and landing locks for the planar array antenna and solar panel. The antenna support structure has three controllable axes; the solar panel is mounted to the antenna support structure by a single controllable axis. The roll-, elevation-, and solar-axis drives each utilize a three-stage planetary gear reduction. The polar-axis drive uses a single-stage planetary and a double enveloping worm gear. Each drive has a solenoid stepper motor for power and a wirewound potentiometer for position indication.

The developmental unit X-1, upgraded to include a strengthened elevation housing, solar panel tube support fittings, and a vibration damper between the solar panel and mast, has completed successful type-approval vibration tests in the $x$- and $y$-axes while installed on the S-2A spacecraft at HAC. The damper reduced the motion of the solar panel and antenna, at the positioner resonant frequency, to within the required dynamic envelope.

An outmoded positioner is being upgraded for use in the thermal-control-model evaluation program. The positioner drive mechanisms are being modified to provide the torque required for operation in the Earth's gravitational field.

## D. Flight Control

### 1. Thrust-Phase System Design

An analog computer study was completed by HAC to define quantitatively the effect of vernier-engine hysteresis on the flight attitude-control and acceleration-control loop performance. The complete three-axis attitude-control subsystem and the acceleration-control subsystem were coupled together because of vernier-engine gain mismatch and the accelerometer center-of-gravity offset effect.

The presence of hysteresis in the transfer characteristic of any or all three vernier engines produces small amplitude limit-cycle motions about the spacecraft pitch and yaw axes. The amplitudes of these motions depend on vehicle inertia, engine gain mismatch, and hysteresis loop width. Quantitative amplitude data were obtained for each of the mission thrust phases. Although further study is required to fully assess the possible degradations to over-all system performance caused by these angular motions, the following conclusions were reached during this study:

(1) Hysteresis-induced limit-cycle modulations of vernier engines have a negligible effect on midcourse correction accuracy (resulting magnitude error of less than 0.06 ft/sec).

(2) Radar noise inputs do not magnify limit-cycle effects. System response from simultaneous action of radar noise and engine hysteresis appears to be roughly the superposition of responses caused by each acting separately.

### 2. Canopus Sensor Tests

Reliability demonstration tests were completed successfully on two flight-model Canopus sensors. Each unit was subjected to 250 hr of preconditioning testing to simulate conditions normally encountered prior to launch. This testing was followed by exposure to 27 mission cycles to reach the reliability objective of 0.97. At the beginning of the first three launch cycles, each unit was subjected to expected launch vibration levels for a period of 12 min. The mission cycle consisted of continuous operation in a vacuum environment at temperatures expected during a mission, followed by a functional checkout of the unit. Both units performed satisfactorily at the completion of the 27 missions. Functional tests of one of the units were successfully completed.

### 3. Automatic Sun Acquisition Studies

In the initial spacecraft design, Sun acquisition and orientation was initiated manually by ground command and took place while being monitored by means of the spacecraft-to-ground telemetry link. Thus, DSIF acquisition was a prerequisite to Sun acquisition. In addition, proper spacecraft thermal control is dependent on proper Sun orientation, and early Sun acquisition is required to establish the proper thermal environment.

Recent concern about the time required for Deep Space Instrumentation Facility (DSIF) acquisition and the possibility of this acquisition being delayed as long as 30 to 60 min has led to several studies regarding the advisability and feasibility of incorporating an automatic Sun acquisition mode that does not require any commands or monitoring by the DSIF. The studies indicate that it is desirable to add a new acquisition Sun sensor which is not affected by other than direct sunlight and which will eliminate the threat of earthlight interference during early Sun acquisition. Placing this unit on the flight-control sensor group would eliminate dependence on previous proper positioning of the solar panel and permit earlier Sun acquisition initiation. Addition of the capability to acquire the Sun automatically would eliminate the threat of temperature extremes as long as Sun acquisition takes place within 60 min after launch. The present secondary Sun sensor should be retained on the solar panel to serve both as a backup for Sun acquisition and for necessary lunar operations.

### 4. Reorientation of Sun Sensor Plane

The acquisition Sun sensor sensitive plane was reoriented to coincide approximately with the spacecraft roll–pitch plane, as shown in Fig. 3. (The center of the sensitive plane is actually offset 1.5 deg from the roll–pitch plane.) For the new configuration, the normal Sun acquisition sequence (following the 51-sec time delay after the separation and legs-down signals) will be a negative roll maneuver until one or both of the sensor cells are illuminated, followed immediately by a positive yaw maneuver until the lock-on cell of the primary Sun sensor is illuminated. Since the second rotation will always be a positive yaw maneuver regardless of which cell is illuminated, some simplification of the electronic logic circuits was possible. (In the previous orientation, the polarity of the second rotation depended on which cell was illuminated.) A single digital telemetry signal will be sent to indicate illumination of the Sun sensor slit.

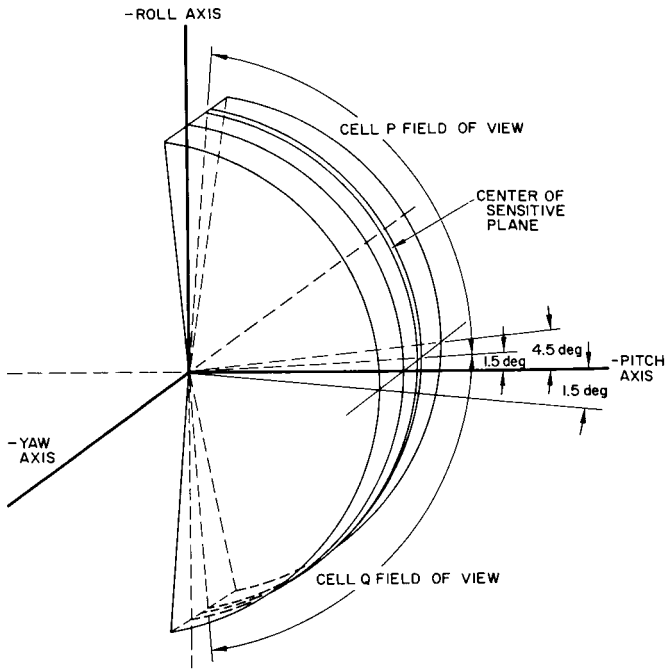


**Fig. 3. Acquisition sensor field of view**

Satisfactory system operation with the new acquisition sequence was verified by an analog computer study. Vibration and performance tests were conducted at HAC on an engineering model of the new sensor configuration. Sensor design has been completed and a detail specification prepared. Flight quality hardware is being fabricated.

### 5. Power Supplies

A study is being conducted by HAC on ways to reduce the over-all spacecraft power deficit by increasing the efficiency of the three-phase power generated by the flight-control sensor group. A 21-v-rms 400-cps three-phase square-wave power supply has been proposed.

The minimum modified square-wave operating voltage of the Canopus sensor motor was determined in the presence of simulated boost acceleration. Three sensors were mounted on a centrifuge and subjected to 10-$g$ acceleration along the thrust axis for 4 min and 5-$g$ acceleration for 7 min. Half-way through each acceleration test, the motor voltage was slowly decreased until the motor stopped. Then the voltage was increased slowly until the motor started. Each sensor motor was also tested three times for stopping and starting voltages with the centrifuge not running. Results of the test indicate that the sensor motor will operate properly during

launch acceleration with the modified square-wave power supply.

Tests to determine the feasibility of operating gyro motors with the modified square-wave power supply were completed. A comparison was made of the performance of five gyros using 26-v-rms 400-cps sine wave and three-phase delayed square wave with the 400-cps fundamental set to 26 and 21 v rms. The effect of spin motor excitation on fixed drift, spin, and input-axis mass unbalance was determined. Differences noted were within the test-to-test variations to be expected. Wheel synchronization and rundown times were measured with the gyros at room ambient temperature and at normal operating temperature (180°F). One gyro was evaluated for runup characteristics at square-wave voltage levels between 26 and 15 v rms. It was shown that the torque available for acceleration of the wheel decreases rapidly at voltage levels below 21 v rms. There is approximately a 45% reduction in excess torque when operating the gyro motor at 21 v rms.

Heater power requirements were found to increase by approximately 0.7 w at 21 v rms because the heater is compensating for the reduced spin motor power dissipation. A change in the gyro transfer function results because the heat generated by the gyro spin motor is more effective than the heater in controlling the damping gap temperature. The gyro transfer function decreased by 1.6% when the spin motor excitation was decreased from 26 to 21 v rms. This is equivalent to a decrease in damping gap temperature of approximately 0.5°F.

Based on the results of these tests, the 26-v-rms three-phase sine-wave power supply will be replaced with a 21-v-rms equivalent square-wave power supply in the flight-control electronics unit. Redesign of the AC electronics control unit and programmer is under way to provide the modified square-wave power supply. Tests on an engineering model of the supply indicated an operating efficiency of approximately 60% into a 10-w load. The spacecraft power deficit can be reduced by approximately 600 w-hr by replacing the sine-wave supply with the modified square-wave supply. The redesign effort in the electronics control unit involves the modification of the wiring harness and one chassis and an addition of another chassis. Modification of the advanced flight-control programmer includes a change of tuning fork, redesign of the 400-cps output amplifiers, and addition of a delay circuit to provide a −90-deg phase signal.

# E. Engineering Experiments

## 1. TV Camera Thermal Study

A redefined survey camera thermal model was used to predict the capability of the camera heaters to bring the camera to operating temperature under worst-case conditions during the transit phase. Initial nodal steady-state temperatures during transit were calculated. Studies of the operation of the survey camera on the Moon's surface during the last few hours of the lunar night are still in process at HAC.

Results of these studies indicate that modifications must be made to the survey camera to ensure that the heaters will be capable of raising the electronics to their minimum operating temperature of −20°F during either transit or lunar night conditions. While these are not requirements of the mission, it is desirable to provide this capability if the penalty is not excessive. It appears that an exterior surface composed of white paint and polished aluminum will make possible camera operation with heaters during the transit and lunar night environments.

A thermal model for the approach TV camera is being definitized. A study was initiated to determine if the individual components of the camera were tested to adequate thermal rates and levels. One component, the deflection yoke, was believed to have been tested marginally. An investigation of the manufacturing techniques and test procedures was initiated, and a test at low temperatures was started. Although the testing has not yet been completed, preliminary results show that the yokes will survive the temperature rate of change and minimum temperature levels expected during the transit and lunar night phases.

## 2. Touchdown Dynamics Experiment

The objectives of the touchdown dynamics experiment are: (1) to determine the linear and angular acceleration, velocity, and displacement of the spacecraft reference axes during touchdown and to express these motions in a lunar inertial reference system; and (2) to obtain information on the bearing strength of the lunar surface, the shearing resistance and/or coefficient of friction of the lunar surface for both static and dynamic conditions, the penetration of the spacecraft into the lunar surface, and lunar surface contours in the landing area. To meet these objectives, the subsystem must be capable of

retrieving, storing, and relaying 21 channels of data developed immediately prior to and during a *Surveyor* landing. The data to be retrieved, stored, and transmitted to Earth by means of telemetry are as follows:

(1) Three mutually orthogonal components of translational acceleration (derived from three accelerometers).

(2) Three mutually orthogonal components of angular velocity (derived from three gyros).

(3) Axial forces in six landing leg struts and three shock absorbers (derived from nine strain gages).

(4) Angular position of each landing leg (derived from three potentiometers).

(5) Initial contact time of each footpad and crushable block (derived from six switches).

An investigation is under way at HAC of the technical problems and program implications associated with the inclusion of the touchdown dynamics experiment in the *Surveyor* payload.

# F. Testing Facilities and Equipment

## 1. Payload Systems Laboratory

Fabrication of the HAC Payload Systems Laboratory test configuration has been completed. This configuration (Fig. 4) consists of the following major elements: scientific instrument test rack, M-13 simulated spaceframe and mounting stand, scientific payload spacecraft harness, junction box assembly, interconnecting cables, test tees, and junction box (spacecraft/test cables). All scientific instruments and auxiliaries have been installed on the M-13 spaceframe. Experiment checkout and integration tests have begun.

## 2. Data Acquisition Center

The increasing work load, which often involves more than one spacecraft undergoing system testing simultaneously, has created the following requirements: (1) increased real-time test control, test monitoring, and data acquisition visibility; and (2) increased capability to perform near-real-time data playback and processing for analysis. To meet these requirements, a data acquisition center conceptual design was completed.

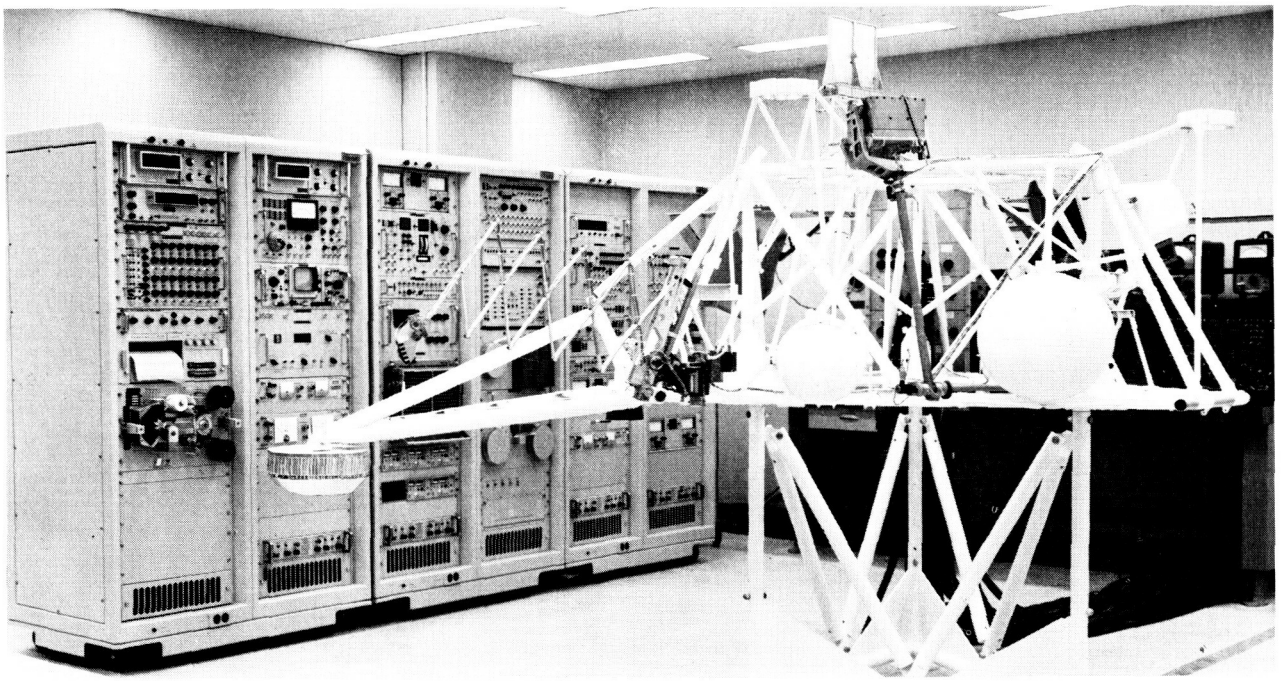

**Fig. 4. Payload Systems Laboratory test configuration with scientific instruments installed**

The facility will consist of two real-time test monitoring and data acquisition stations, one off-line data playback and editing station, and a data analysis station which will support both the real-time and off-line functions. Adequate digital data analysis equipment will be utilized to properly sort, scale, and limit-check the telemetry and hard-line data. The output format of the data to the analysis station will assure that quick-look and detailed analyses can be performed promptly during test operations.

The development of the data acquisition center is planned in two phases: The first-phase installation will consist of one command and data handling console and peripheral equipment, augmented with four tape recorders, a command decoder, and a time code translator; the second phase will include digital data analyzers, additional telemetry processing equipment, and more extensive data displays.

### 3. *Surveyor Management Computer Programs for Processing of System-Test Telemetry Tapes*

One of the major objectives in the development of engineering management computer programs (Fig. 5) is the processing of system-test spacecraft data. The engineering management computer programs necessary to perform a complete analysis of these data are: (1) an engineering data reduction program, (2) a sequence translator program, (3) a power management program, and (4) a thermal management program.

System-test telemetry data will consist of a command sequence tape (composed of commands given to the spacecraft, each with an associated time in order of increasing time) and a spacecraft telemetry tape (composed of frames of actual spacecraft data corresponding to the sequence of commands contained in the command sequence tape). The spacecraft telemetry tape will be processed in the engineering data reduction program. The processed data, i.e., power and thermal data tables, will be in a form acceptable by the power management and thermal management programs, respectively. The command sequence tape will be reformatted by the sequence translator program (including only those commands which affect the spacecraft power subsystem) into a form acceptable to the power management program.

The power management program uses the processed command sequence and spacecraft telemetry tapes to predict values of spacecraft telemetry data points as a function of the command sequence, to compare predicted values with actual values at equivalent times in the command sequence, and to record important power subsystem parameters such as battery energy. After each command, the power management program will compute the values of power subsystem parameters, including most spacecraft telemetry data points, and compare the computed values to the actual values from the power data table.

The power management program outputs dissipation information for use by the thermal management program in the power dissipation table. The thermal management program uses this information and the thermal-data-table temperature data points to output temperatures of power subsystem elements and heater temperatures for use by the power management program.

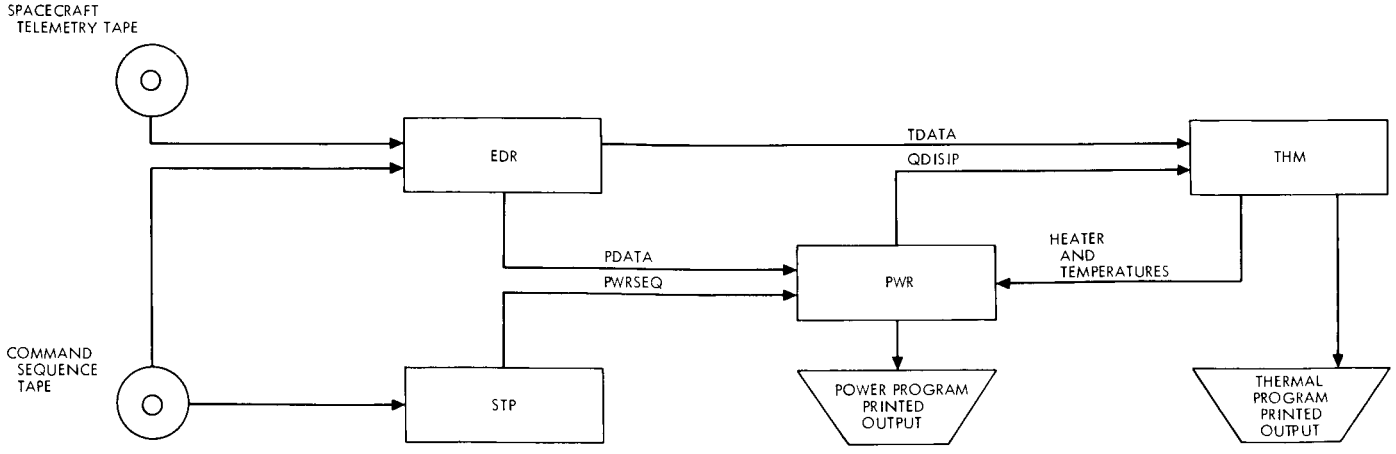


**Fig. 5. Engineering management computer program interface**

### 4. System-Test Equipment

Vibration testing of stray energy monitors was conducted at HAC to verify mechanical survivability under expected spacecraft vibration levels. Three tests on each of the three major axes were performed on 29 units. Three mechanical activation-type failures occurred, all at levels in excess of 30 $g$. It is believed that these failures were random in nature and that a confidence level of about 95% could be attained if a preconditioning vibration test was performed on each device before actual test use. This test would remove marginal units before installation on the spacecraft. Should an activation occur during spacecraft vibration testing, microscopic examination at the end of the test would reveal the cause of activation (either mechanical or electrical).

# PLANETARY–INTERPLANETARY PROGRAM

# III. *Mariner* Project

## A. Introduction

The early objective of the Planetary–Interplanetary Program is the initial probing of the planets Mars and Venus by unmanned spacecraft. The initial probing of Venus was successfully accomplished by *Mariner II*. The next operation directed toward this objective is the initial probing of Mars by the *Mariner IV* spacecraft which is now in transit.

The primary objective of the *Mariner C* missions (*Mariner* Mars 1964 Project) is to conduct closeup (flyby) scientific observations of the planet Mars during the 1964–1965 opportunity and to transmit the results of these observations back to Earth. The planetary observations should, to the greatest practical extent, provide maximum information about Mars. TV and cosmic dust experiments and a reasonable complement of field- and particle-measuring experiments are being carried by *Mariner IV*. In addition, an Earth occultation experiment is planned.

A secondary objective is to provide experience and knowledge about the performance of the basic engineering equipment of an attitude-stabilized flyby spacecraft during a long-duration flight in space farther away from the Sun than the Earth. Field and/or particle measurements will be made in interplanetary space during the trip and in the vicinity of Mars.

The *Mariner C-2* (*Mariner III*) spacecraft was launched from the Air Force Eastern Test Range (AFETR) on November 5, 1964, at 19:22:04.920 GMT after a 1-day delay. Due to a malfunction of the spacecraft shroud, the spacecraft solar panels did not deploy. The launch of *Mariner C-3* (*Mariner IV*) was delayed while the *Mariner III* failure was analyzed and a new shroud designed. *Mariner IV* was launched from the AFETR on November 28, 1964, at 14:22:01.309 GMT. All launch vehicle and spacecraft events were very close to nominal. The spacecraft is performing as designed with all subsystems operating properly (except for the solar plasma probe discussed later in this section); at the end of this

reporting period, the spacecraft had operated for about 800 hr of its 6000-hr mission life.

*Mariner C-1* (*Mariner* proof test model) was used to support the preflight operations of *Mariners III* and *IV* and the investigations of the *Mariner III* flight failure. It is now being used to support the *Mariner IV* flight analysis effort. The *Mariner C-4* (backup) spacecraft was further tested and assembled to complete flight configuration to support the *Mariner IV* prelaunch, launch, and postlaunch activities.

## B. Mission Operations

### 1. Mariner III (Mariner C-2)

The *Mariner III* launch scheduled for November 4 was delayed 1 day to allow more time to analyze an *Agena* velocity meter relay problem and to further review the down-range S-band instrumentation status. The spacecraft was launched from the AFETR on November 5 at 19:22:04.920 GMT. The fiberglass aerodynamic shroud failed to eject from the spacecraft, and, although the vehicle performance was very nearly nominal, the added weight of the shroud resulted in a short-range orbit with a closest approach distance to Mars of 42,000,000 mi and a period of revolution of 448.7 days. With the shroud still covering the spacecraft, the solar panels could not deploy and the only source of power was the on-board battery, which kept the subsystems operating until 04:05 GMT on November 6.

Several commands were transmitted to the spacecraft during the 8-hr, 43-min period of battery life in an attempt to determine and confirm the failure mode of the vehicle. Efforts were made to fire the midcourse propulsion motor in an attempt to free the spacecraft from the shroud, but battery power was depleted before the maneuver could be executed.

### 2. Mariner IV (Mariner C-3)

The spacecraft was moved to the launch pad, and the first part of the JPL simulated countdown was completed on October 31. Several problems were detected and resolved within the operational support equipment (OSE), but the spacecraft experienced no difficulties. On November 3 the spacecraft power was turned on, and no problems with the spacecraft or OSE were detected.

Due to the flight failure of *Mariner III*, the *Mariner IV* spacecraft was demated from the *Agena* on November 6 and moved to the explosive safe facility (ESF). The shroud was removed, but the spacecraft was not demated from the adapter. The spacecraft–adapter combination was then placed under protective cover, and constant dry-nitrogen purge was maintained. The *Mariner IV* shroud was returned to Lockheed Missiles and Space Company (LMSC). An emergency effort was undertaken by Lewis Research Center and LMSC, and a new magnesium–thorium shroud was designed, fabricated, and tested at LMSC.

Two joint flight-acceptance composite tests were conducted on the launch vehicle only. Complete launch pad checkouts were performed to support the new launch day of November 27. All blockhouse equipment was found to be functioning normally. The spacecraft simulator was used to check the ESF electrical complex before connections to the spacecraft were made.

The new shroud was delivered to the AFETR ready for flight on November 22. To compensate for the added weight of the metal shroud, the command destruct system and the retrorockets were removed from the *Agena* vehicle. The shroud was installed on November 23, and a surface contact measurement was made between the adapter and shroud surfaces; 95% contact was measured, which eliminated the necessity for any scrapping operation. The separation spring alignment was verified, and no alignments were necessary.

With the shroud installed on the spacecraft, the separation spring stroke and preload were measured. Adjustments were made and the shroud was mated for the last time. The shroud V-band torquing was completed on November 24 without incident. During the shroud leak test, the leak rate was found to be excessive. Adjustments were made on the door and, in addition to obtaining complete latching for all door positions, an excellent pressure seal was obtained.

Final electrical checks were made at the ESF, and the spacecraft was moved to the launch pad and mated with the *Agena* on November 24. The cooling blanket was installed the following day, and voltage, no-voltage checks were made on the umbilical before connecting it to the spacecraft. The spacecraft power was turned on

and the first part of the countdown was started, with the objective of performing the most detailed spacecraft verification permitted within the limits of the launch pad environment.

On November 27 at $T - 220$ min, the spacecraft joined the launch count. Spacecraft power was turned on at 09:37 GMT. The launch effort was terminated at $T - 60$ min due to a problem in the S-band radio spacecraft–system-test-complex system. Troubleshooting and data analysis of the S-band problem continued after the termination of the countdown. Based on the results of exhaustive testing, worse-case analysis, and range scheduling, the second launch attempt was scheduled for November 28, with a $T - 0$ at 14:22 GMT. The spacecraft countdown started at $T - 230$ min at 09:22 GMT, and the spacecraft was placed on external power at 09:32 GMT.

On November 28 at 14:22:01.309 GMT, *Mariner IV* was launched from the AFETR. There were no unscheduled holds. All launch vehicle and spacecraft events were very close to nominal, resulting in a successful Mars encounter orbit with a spacecraft–Mars miss distance of approximately 150,000 mi.

A successful midcourse maneuver was performed December 5, with the resultant flyby point only approximately 1000 km from the aiming point. This is well within the "highly desirable" zone for the science experiments. The closest approach to the surface will be about 5060 mi.

On December 6 the solar plasma probe developed a problem which may render any further data from that instrument useless; the cause of this problem is not yet thoroughly understood. All other subsystems are operating properly.

On December 13 a command was transmitted to the spacecraft to transfer from the S-band cavity amplifier to the S-band traveling wave tube. This tube is capable of slightly more power output and has shown evidence of much longer life. It was not possible to launch with the tube turned on due to potential arcing of its high-voltage circuits during the launch phase.

On December 17 a command was transmitted to the spacecraft to remove certain sensitivity limits associated with the Canopus tracker. This was necessary to ensure against occasional losses of Canopus lock.

### 3. *Mariner Proof Test Model (Mariner C-1)*

The proof test model supported the JPL Space Flight Operations Facility (SFOF) testing during this reporting period. Spacecraft telemetry data were transmitted to the SFOF by teletype. Various spacecraft failures were simulated to give SFOF personnel an opportunity to analyze non-standard telemetry data. They, in turn, evolved analysis and took corrective action by means of the command subsystem whenever possible.

Immediately preceding the launch of *Mariner III*, the proof test model was put in a full-flight support configuration and connected to its related system test complex. During the launch and postlaunch phases, various effects of the apparent non-separation of the shroud from the *Mariner III* spacecraft were simulated, including operation of the system at a low bus voltage, the interaction between attitude-control gas valve operation and that of the magnetometer (in the "panels up" configuration), and spacecraft free-mode operation during exposure to sunlight (again in the "panels up" configuration).

During the preliminary steps for vibration, difficulty was encountered in locking the spacecraft receiver to the ground test transmitter. (The automatic phase control readout indicated a displacement from the normal no-signal condition, and the telemetry automatic gain control indicated an input signal whether the test transmitter was on or off.) It was found during testing of the radio that, when the ranging receiver was on, an internal lock condition could occur. It was decided to modify the countdown procedure to delete the use of the ranging receiver in the transponder.

Additional tests were conducted to help resolve some spacecraft behavior characteristics observed during the *Mariner III* flight.

In support of the *Mariner IV* mission, a midcourse maneuver was conducted during the postlaunch phase of a system verification test to confirm the capability of the OSE and spacecraft to perform the maneuver and to provide practice for the SFOF operations team. A test on December 3 verified that the SFOF tapes for midcourse maneuver commands were of proper duration and polarity.

A special test was performed to determine why the spacecraft lost lock on Canopus after the command was

sent to initiate the midcourse maneuver sequence. Various power-change transients and roll error values were used in an effort to put the Canopus sensor out of track, but the sensor did not lose lock at any time.

On December 11 a plasma probe test was conducted to observe the effects of the noise due to high-voltage arcing on the science data automation system and data encoder. The science data automation system lost sync, and the data encoder skipped on the 200-deck segment of the commutator. Radio and attitude control were not affected.

### 4. Backup Spacecraft (Mariner C-4)

The *Mariner C-4* spacecraft was maintained and tested at the AFETR as a set of flightworthy spares and as a backup to *Mariner IV* after the failure of *Mariner III*.

An attitude-control leak test was performed on *Mariner C-4* at the ESF between October 28 and November 2. The spacecraft was then returned to Hangar AO, and all missing hardware was installed. The spacecraft was put in a ready state to support any investigation during the launch or postlaunch phases of the *Mariner III* mission.

After the launch of *Mariner III*, the *Mariner C-4* backup spacecraft was placed in a full flight configuration to maximize the probability of meeting the launch period constraint for *Mariner IV*. On November 10 the spacecraft power was turned on, and a system verification test was performed. The only difficulty experienced was with the cosmic ray telescope. Alignment checks were performed on the TV subsystem and scan platform.

Science calibrations were completed November 12. The trapped radiation device, ion chamber, plasma, and magnetometer checks were also performed at that time. From November 13 to 17, system testing was conducted, including the magnetometer current loop measurements; all measurements were within tolerance. Magnetometer mapping was performed on November 18.

Final mechanical preparations were completed on November 20. Two updated type-approval solar panels were inspected, sunlight-tested, and assembled to the spacecraft. The final mechanical buildup was completed November 24, and weight and center-of-gravity measurements were then made. The spacecraft was mounted on its transporter with protective cover installed and was prepared for movement to the ESF, if necessary.

## C. Power Subsystem Operation During the *Mariner* Missions

### 1. Mariner III Mission

*a. Verification of shroud problem.* The strongest supporting evidence for the absence of proper shroud separation given by the power subsystem data was the lack of solar panel and standard cell currents and voltages. Telemetry event counter readings just after spacecraft–*Agena* separation showed that proper firing currents had been delivered to the panel squibs, but no panel deployment was observed. Panel currents moved from a zero-current reading at only one point during the flight.

The lack of panel currents could be explained in three ways: the solar panels were covered with the shroud, the solar panels did not deploy even though squib firing currents were seen, or the solar panels deployed but were facing away from the Sun. Attitude-control spacecraft position indications ruled out the last possibility. In order to verify that solar panel currents would be observed without the shroud but with the panels folded, a special test was performed using the proof test model. With the solar panels latched in the launch configuration, the shroudless spacecraft was rotated to various Sun angles. It was found that only a small illumination was required to raise at least one solar panel to a higher current, and still higher currents could be obtained with the Sun shining directly on one panel. Therefore, the only logical explanation for the lack of panel currents was that the shroud remained over the panels.

At 01:47:40 and 01:47:44 GMT, two solar panels showed currents of 0.79 and 0.47 amp, respectively. Adjoining samples in the data stream looked satisfactory. It is possible that these readings could result if the Sun shone onto the shroud from the rear and reflected from the polished nose onto the panels. No other suitable explanation of these two data points has been found.

According to temperature analysis, the solar panel temperatures observed are those that would be expected with the shroud in place. Although the temperatures observed could be obtained with the panels closed and the shroud removed, they could only exist for one particular spacecraft–Sun orientation. Attitude-control data indicate that the spacecraft was moving in a manner that would not maintain a constant spacecraft–Sun orientation.

*b. Subsystem operation during the mission.* All power subsystem elements performed as expected. Commands

in which the power subsystem was involved were executed properly, and no anomalies were noted.

All inverters and regulators performed properly. The efficiencies of the 2400-cps main inverter and the main regulator were checked and found to agree with the values calculated during system tests. Proper operation of the 400-cps one-phase inverter was verified by movement of the science scan platform when *encounter science* was turned on. (It was possible to confirm from the raw data that the tape recorder was operating as expected from the 400-cps one-phase inverter during the encounter phase.) Operation of the power synchronizer and the 400-cps three-phase inverter was verified by obtaining gyro operation throughout the flight.

Proper operation of the battery charger in the charge mode was partially verified during the flight. Since the solar panels were never available to provide battery charger power, a positive analysis was not possible. It was possible, however, to say that the charger operated as expected, under the circumstances, by taking power from the downstream side of the battery blocking diode and transferring it to the upstream side. Boost-mode battery charger operation was also observed as expected during the flight when the inhibit signal from *gyros on* was removed and Direct Command 28, *battery charger on,* was not in effect.

The actual flight temperatures of the conversion equipment were normal for the operating mode of the spacecraft. Also, all voltage readings were normal for a good *Mariner* battery. Spacecraft power subsystem loadings agreed closely with prelaunch system-test data.

The battery temperature rose from 67°F before launch to a steady 106 to 108°F 5 hr after launch. Normal Earth cruise temperature while charging on solar panel power was expected to be about 85°F. Normal internal heating while discharging caused the higher temperature.

Battery capacity was 53 amp-hr with battery voltage above 25.8 v. An additional amp-hr was obtained before data transmission stopped. Due to some uncertainty in the *Mariner III* battery charger boost-mode conversion efficiency and the lack of every telemetry data point, the accuracy of the battery capacity is ±3 amp-hr. During flight-acceptance testing, this battery gave 50.3 amp-hr on discharge and accepted 56.2 amp-hr on recharge. The higher-than-expected battery capacity was due in part to the high battery temperature. The flight operation of the battery appeared normal in every respect.

### 2. Mariner IV Mission

All elements of the power subsystem performed satisfactorily during the first 15 days of the *Mariner IV* flight. Operation of the conversion equipment was normal for all parts of the launch-through-midcourse sequence. The output voltage from the 2400-cps main inverter remained well within specification. Temperatures of the conversion equipment Bays I and VIII are highly acceptable values and should lead to extended conversion equipment life. Spacecraft power subsystem loading values agree closely with prelaunch system test data and are a further confirmation of proper spacecraft operation.

During the *Mariner IV* launch, the battery supplied spacecraft power for about 68 min; approximately 8 amp-hr of battery capacity was used, including that used during prelaunch testing. While battery power was being utilized, battery voltage was 27.5 to 27.8 v. Upon solar acquisition, battery charging began immediately at 0.250 amp and 28.9 v. After 6 hr, battery voltage rose to 34.0 v and the charge current decreased to 0.050 amp. After 5 days, battery voltage slowly rose to 34.8 v and charge current slowly decreased to about 0.010 amp. These values then remained constant and are not expected to change for several weeks. (Battery power was not used during the midcourse maneuver on December 5; spacecraft power was furnished continuously by the solar panels.)

The battery temperature rose from 67°F before launch to 88°F 10 hr later and then slowly decreased to a stable 75 to 76°F in another 12 hr. During the midcourse maneuver, the temperature rose to 81°F and then decreased to 75 to 76°F within 10 hr. Battery temperature will decline during the cruise mode and may reach 55°F at Mars encounter. These temperatures are quite favorable for extended battery life and yet are high enough for excellent battery operation if needed.

## D. Developmental and Testing Activities

### 1. Precision Wideband Signal/Noise Mixer

Telemetry and command systems and equipment are most meaningfully tested by measuring their performance (e.g., error rate) in an instrumented noisy environment;

thus, devices must be provided to linearly add signal voltages to noise voltages in precisely measured ratios. Audio signal/noise mixers are usually used with telemetry and command systems to avoid the uncertainties and poor measurement accuracies involved with RF carriers. Signal/noise mixers of various degrees of complexity and precision were built to accomplish performance tests at JPL. Some of these performed adequately, but there was uniform agreement among users that a need existed for a new unit, to be designed for the utmost in precision and flexibility.

A new instrument (Fig. 1) has been developed for use at the Deep Space Instrumentation Facility stations and in telemetry and command laboratories at JPL for testing and evaluation of communications (modulation/demodulation) equipment. This signal/noise mixer permits measurements at accuracies and stabilities not previously available in production equipment. Its first operational use is the periodic performance testing of the *Mariner C* telemetry demodulator during the *Mariner IV* mission.

## 2. Propulsion System Life Storage Test

In compliance with requirements for long-duration testing outlined in the type-approval specification for the *Mariner C* postinjection propulsion system, a propulsion system underwent a life storage test at the Edwards Test Station. This test proved that the system could be stored for prolonged periods of time prior to test firing and that the system total impulse was repeatable within the required limits. It was indicated, however, that compatibility of the fuel tank bladder and hydrazine can become a problem if the temperature environment in flight approaches 120°F.

## 3. Mariner High-Voltage Test Program

An electromagnetic interference (EMI) high-voltage test program was conducted to determine if the generation of surface charge on a rocket-propelled vehicle and/or subsequent interaction of this surface charge with the launch environment could function as a mechanism for spacecraft performance degradation. The *Mariner C* high-voltage program was a continuation of similar investigations stemming from the *Ranger VI* failure.

Special EMI high-voltage tests were conducted on the *Mariner C* structural test model (STM) and proof test model (PTM). A test mockup consisting of an *Agena* forward equipment rack mockup, a *Mariner–Agena* adapter ring, the *Mariner* STM, and a *Mariner C* honeycomb-type shroud was assembled on an insulated test stand (Fig. 2). A high-voltage DC generator was arranged to drive the potential of the test assembly with respect to

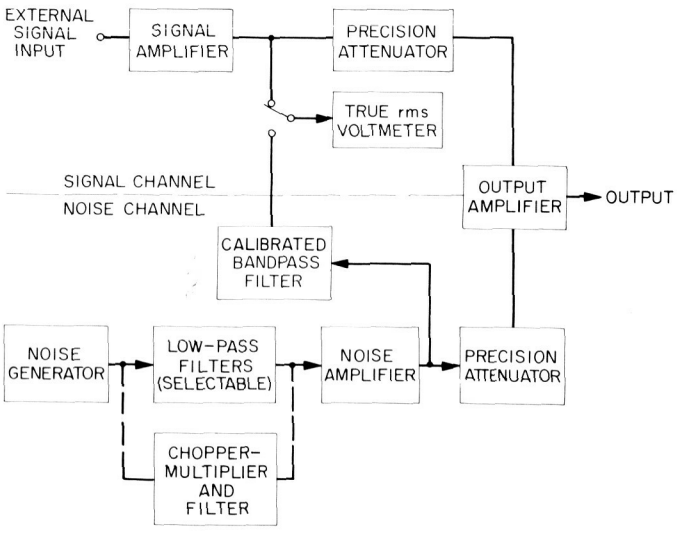


**Fig. 1. Precision wideband signal/noise mixer**

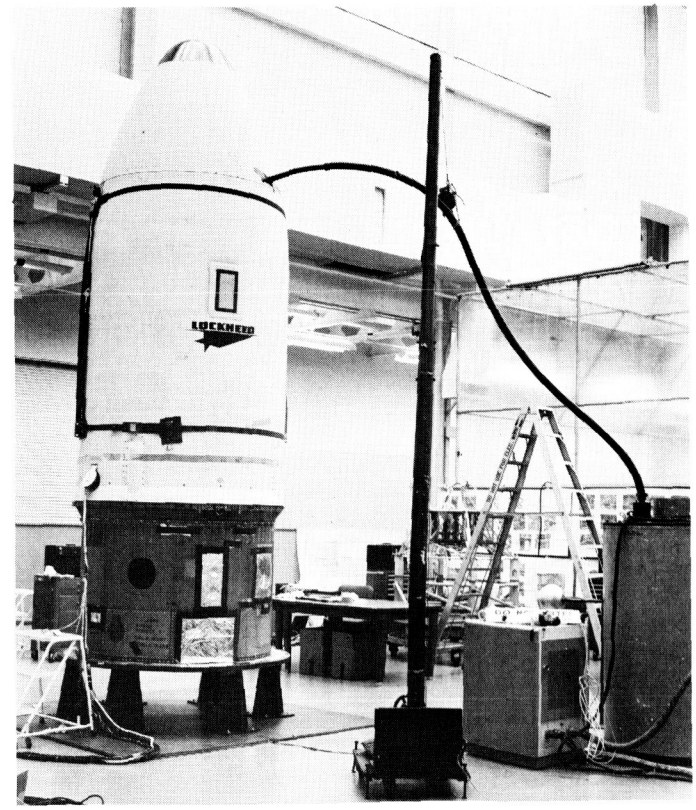

**Fig. 2. EMI high-voltage test configuration**

Earth ground. The test assembly was instrumented with various passive test elements placed about the STM internal to the shroud. A battery-powered oscilloscope was mounted inside the *Agena* forward equipment rack mockup and provided with a viewing port. The assembly was then charged to various potentials and allowed to discharge to Earth across an arc gap of controlled length.

Due to limitations imposed by the current-delivering capabilities of the generator, no charge-induced transients of observable magnitude were expected or found. Arc discharging, however, produced internal transients on the order of 100 to 200 mv for breakdowns from a nominal 100 kv. These transients were of the predicted polarity and wave shape (exponential decay).

The PTM was then placed in the same test mockup, replacing the STM. The PTM test assembly simulated actual launch configuration as closely as was practicable. Live batteries, type-approval solar panels, and live pyrotechnics were installed. Sufficient OSE for operation and checkout of the *Mariner C* PTM was assembled. The PTM was placed in launch mode, all cables were removed, two-way RF link was established, and a calibration round of all deck telemetry was recorded and examined to verify correct operation. High voltage was then impressed on the test assembly in a sequence of 30, 90, 125, and 150 kv. The test assembly was allowed to break down several times to the discharge sphere for each breakdown potential. Following each set of discharges, one round of high- and medium-deck telemetry was recorded and examined. Upon completion of the high-voltage tests, a final round of all deck telemetry was recorded and examined.

Comparison of the calibration and final rounds of telemetry indicated that the high-voltage discharging of the shroud had no effect on the PTM. Real-time monitoring of the RF link gave no indication of temporary degradation or failure of the system.

# DEEP SPACE NETWORK

# IV. Deep Space Instrumentation Facility

## A. Introduction

The Deep Space Instrumentation Facility (DSIF) utilizes large antennas, low-noise phase-lock receiving systems, and high-power transmitters located at stations positioned approximately 120 deg around the Earth to track, command, and receive data from deep space probes. The DSIF stations are:

| Station | Location |
|---|---|
| Goldstone Pioneer | Goldstone, California |
| Goldstone Echo | Goldstone, California |
| Goldstone Venus (R&D) | Goldstone, California |
| Goldstone Mars (Advanced Antenna System; under construction) | Goldstone, California |
| Woomera | Island Lagoon, Australia |
| Canberra (under construction) | Canberra, Australia |
| Johannesburg | Johannesburg, South Africa |
| Madrid (under construction) | Madrid, Spain |
| Spacecraft Monitoring | Cape Kennedy, Florida |

To improve the data rate and distance capability, a 210-ft antenna is under construction at the Goldstone Mars Station, and two additional antennas of this size are scheduled for installation at overseas stations. Overseas stations are generally operated by personnel of the respective countries.

It is the policy of the DSIF to continuously conduct research and development of new components and systems and to engineer them into the DSIF to maintain a state-of-the-art capability.

## B. Tracking Stations Engineering and Operations

### 1. Pioneer Station

Prior to the launch of *Mariner III*, the Pioneer Station participated in the first mission simulation test. Attempts to acquire the *Mariner III* during the first view period after its launch on November 5 were unsuccessful. Additional system testing was conducted before the launch of *Mariner IV*. Practice countdown exercises were conducted by station personnel to verify continued operational readiness.

Following the launch of *Mariner IV*, the Pioneer Station attempted to "hear" the spacecraft as it went into the injection orbit, but the terrain features at the station raised the eastern horizon too high to accomplish the reception. First acquisition of the spacecraft occurred late in the evening of November 28. Canopus lock was delayed until November 30 when the Woomera Tracking Station had already taken over tracking operations of *Mariner IV*. The commands which caused the Canopus sensor to unlock from other stars were initiated by the Pioneer Station.

Two midcourse maneuvers were initiated. The first, which occurred on December 3, was inhibited almost immediately when the spacecraft performed an unscheduled roll. The second, on December 4, successfully completed the midcourse correction. Scientific, engineering, and cruise-mode data are being recorded in near-real time.

The S-band system for the Madrid Station was assembled and tested in late December at the Pioneer Station. With the Pioneer Station 85-ft antenna in full use for *Mariner IV* tracking operations, all future tests of the Madrid S-band system involving the antenna will be performed after its delivery to Madrid in early 1965. The S-band system for the Spacecraft Monitoring Station is being partially assembled and tested at the Pioneer Station. The equipment will be shipped to the Air Force Eastern Test Range in early 1965, and final assembly and complete system testing will be performed there.

## 2. Echo Station

During November and the first two weeks of December, Echo Station personnel contributed full support to the Pioneer Station for the launch of *Mariner III* and the launch and tracking of *Mariner IV* until the midcourse maneuver was completed. Because the L-band system was being held in a standby condition since the completion of the *Ranger VII* mission, the time was used to recable the 85-ft antenna and to perform cone testing of the Madrid S-band cassegrain cone. In addition, star track tests were performed with a radiometric cassegrain cone under development.

In December preliminary L-band system testing was begun. Cable loss calibrations of the new cabling installed on the antenna were completed. During the last two weeks in December, operations personnel were withdrawn from the *Mariner* mission to complete the L-band system preparations for the *Ranger C* systems and operational readiness tests scheduled for early 1965.

## 3. Venus Station

The exciter for the *Mariner C* 100-kw cassegrain cone transmitter was installed in the Venus Station control room. System tests of the exciter and transmitter are under way, including ground testing of the cone transmitter and antenna testing with full 100-kw capability. A modification to provide a receiving capability in addition to the transmitting capability is currently being installed and tested.

A new 2388-Mc cassegrain cone (Fig. 1) has been constructed to replace the cone which had been damaged in September 1964. Several major improvements were made:

(1) The 100-kw transmitter, water load, and transmitter water-load switch were placed inside the cone.

(2) The previous maser package was rebuilt with a DSIF configuration, incorporating a helium load in the maser cryogenic assembly.

(3) The nitrogen-load vacuum Dewar was replaced with a long-life foam unit.

(4) The post maser receiver and monitor receiver were integrated into one unit.

(5) A quick-disconnect capability was built in to allow rapid changeover to the *Mariner C* 100-kw transmitter cone.

A continuing program of S-band radar experiments on the planets Venus and Jupiter has been carried on during their respective view periods. The Venus tracking experiment, now concluded, produced high-accuracy and precision data for over 2 mo and aptly demonstrated the capabilities of the system. The data obtained are being used to determine the Venus backscattering law and, in conjunction with previous tracking data and all available doppler data, to better determine various astronomical constants used in orbit calculations for Venus and Earth. The primary purpose of the present experiment is to detect reflected signals from the planet Jupiter. All spectra obtained from a particular segment of the surface of Jupiter will be averaged together in an attempt to detect a returned signal.

Successful ranging of the Moon was accomplished at the Venus Station with the X-band lunar radar system.

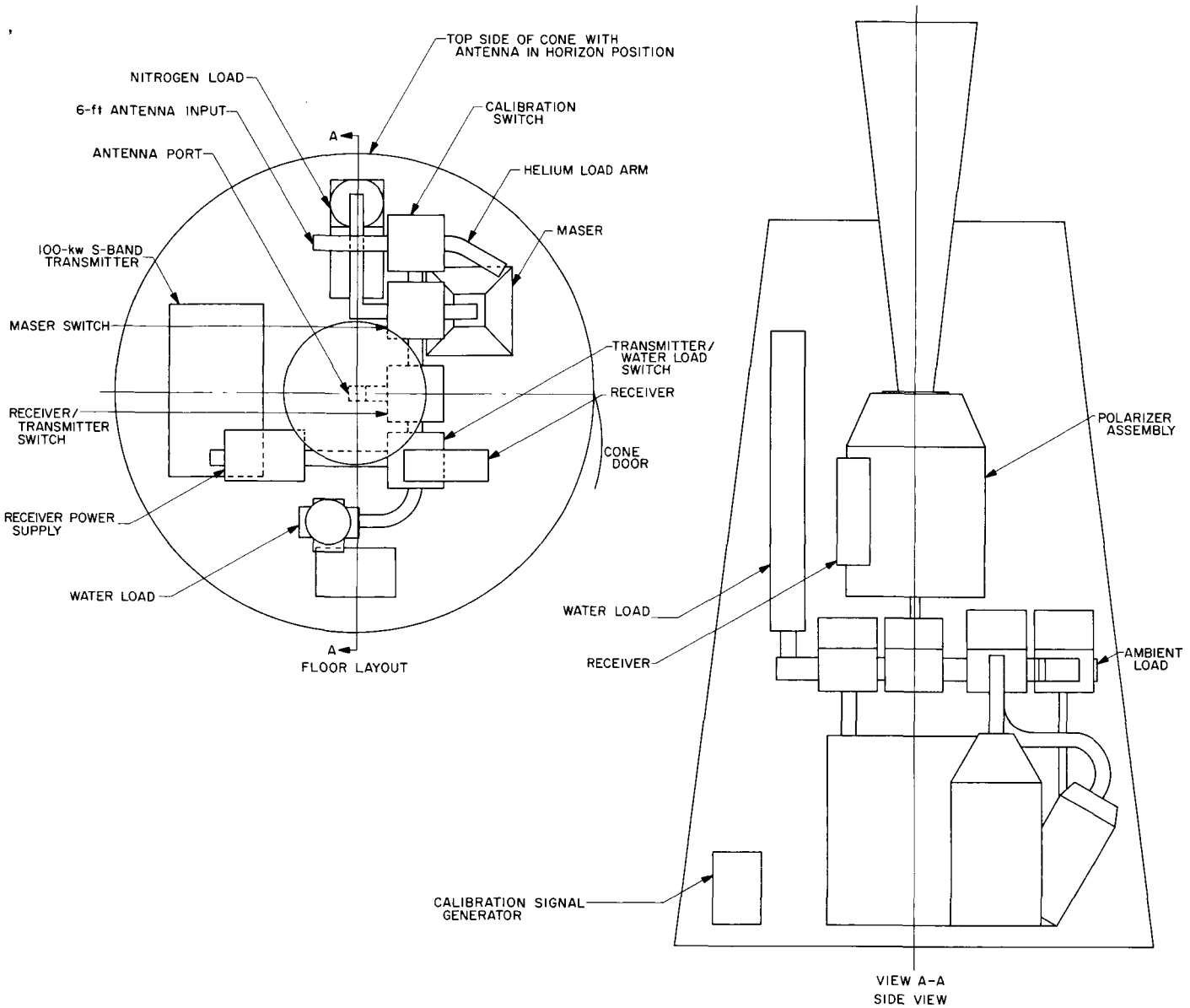


**Fig. 1. Redesigned cassegrain cone**

About 3.5 to 4 hr of ranging data were accumulated, and preliminary analysis indicates an improvement of 10 to 14 db in signal-to-noise ratio as compared to that obtained with the S-band system. Further refinements in the system will result in an additional improvement of at least 3 db. Thermal radiation measurements of the Moon made using the X-band system yielded an average measured temperature of 120°K as defined at the maser input.

Optical and radio star tracks are being made with the S- and X-band radar systems to check the performance of their respective antennas. Also, radiometer experiments at 23 Gc are being conducted on the 30-ft antenna. The primary observation is of Jupiter, but the Sun and radio star sources are also observed for calibration purposes.

### 4. Canberra Station

Construction of the Canberra Station 85-ft polar-mounted antenna (Fig. 2) was completed November 6, thus bringing the station closer to operational status. This antenna incorporates all the new DSIF features embodied in the recent retrofit program (e.g., new declination cage, truss quadripod, counterweight cages, air conditioning, and acquisition aid subsystem). Also, the following improvements were incorporated in the new

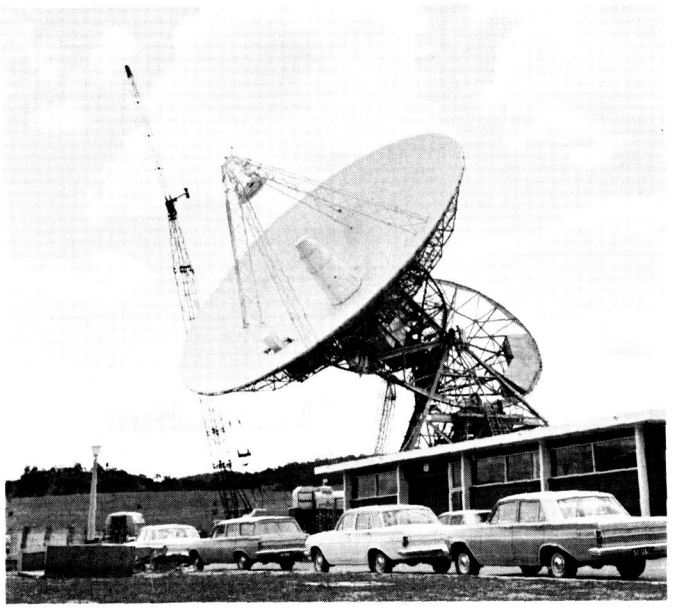

**Fig. 2. Canberra Station 85-ft polar-mounted antenna**

antenna: new high-performance S-band surface panels, increased hour angle coverage, a four-legged pedestal, a structure designed for improved surface tolerance and general stiffness, and modified hour angle and declination drive skids for adjustability and improved stiffness.

# C. Developmental and Testing Activities

### 1. First Pass Acquisition Procedure Tests

Tests were made to develop and prove an acquisition procedure which would achieve the following objectives in the shortest possible time after a spacecraft appears above the local horizon: (1) good two-way doppler data condition, (2) good telemetry data condition, and (3) good angle data above a 10-deg elevation angle. A helicopter carrying a standard DSIF transponder was instructed to fly a special flight profile which resulted in an angular tracking rate at the DSIF of approximately 0.05 deg/sec, and to repeat this course 500 or 1000 ft to the east or west of a predetermined "on-line" course as instructed. The on-line course corresponded to the nominal predicted spacecraft track over the station, and the 500- and 1000-ft courses corresponded to approximately 5.5 and 11 deg relative to this line at the horizon.

On several of the runs, the "apparent" frequency received from and sent to the transponder was biased to provide the operators an opportunity to search for a new frequency on each run. A time bias was also introduced on some of the runs where the first event was called prior to the actual occurrence of first visibility. Transponder automatic-gain-control voltage was called by the pilot immediately as up-link lock was obtained.

The tracking data handling subsystem and the analog portion of the station instrumentation subsystem recorded all station performance data required to evaluate the acquisition time under the various conditions of the test. Angle tracking was accomplished on all runs on which two-way lock was first achieved. Auto-track on the spacecraft acquisition aid (SAA) was accomplished as soon as the helicopter reached 10 deg above the horizon (average time: 154 sec; average rate: 0.06 deg/sec), and auto-track on the S-band cassegrain monopulse (feedhorn and bridge system; SCM) was achieved shortly afterward (average time: 35 sec).

The following conclusions were drawn from the data obtained during these tests: (1) The time from first visibility to two-way lock on the SAA depends strongly on both up-link and down-link signal strengths; (2) flight path variations and transponder frequency offsets do not exert a strong influence on two-way lock time; and (3) two-way lock can generally be achieved in the following times from first visibility: 12 sec minimum, 136 sec maximum, and 50 sec average. The acquisition procedure was shown to provide good doppler data at the earliest possible time after first visibility, reliable auto-track at 10 deg above the horizon, and good angle data some 35 sec later.

### 2. Mariner IV Carrier Lock Verification Procedure

A simplified operational procedure has been developed for detecting and correcting carrier lock on a telemetry sideband. A 70-cps R-C low-pass filter was inserted, by means of a tee, into the telemetry video output line of the Goldstone Duplicate Standard S-band receiver. The filter consisted of a 100-kΩ resistor and a 0.33-$\mu$f capacitor mounted between two coaxial connectors. This filter is high-impedance and causes negligible loading on a telemetry output. The output from the filter was connected to an oscilloscope with the vertical sensitivity set at 0.2 v/cm and the sweep speed set at 20 msec/cm.

If the receiver is locked to the carrier, the telemetry video output contains the telemetry subcarrier frequency

only, which is much higher than the filter cutoff frequency, and the oscilloscope shows only noise. If the receiver is locked to a telemetry subcarrier sideband which is being biphase-modulated at a rate of 33⅓ bps, the video output contains the biphase-modulation rate which is passed by the filter and presented on the scope. This technique allows the detection of sideband lock down to receiver carrier power levels of 15 db above threshold.

### 3. Station Control and Monitor Console

A prototype station control and monitor console (Fig. 3) was installed at the Pioneer Station interim S-band facility building. It is composed of five equipment racks with accommodations for standard 19-in. display, control, and communications panels to be mounted above the desk top (approximately 9-ft over-all length) and can accommodate either a two- or three-man operation. The electronics control and power units and connector patch panels are located in the lower part of the five bays.

Production of the consoles has begun. However, several changes will be incorporated in future units: e.g., a decrease in console height to 45 in. to provide better visibility for the station manager, an increase in the depth of the desk surface to 21 in., and revisions in panel nomenclature to provide a better understanding of switch identification and functions.

### 4. Programmed Local Oscillator

Several changes have been made in the programmed local oscillator used in the planetary and lunar radar experiments at the Venus Station since its original installation in spring 1963. A block diagram of the oscillator incorporating these changes is presented in Fig. 4. The second offset voltage-controlled oscillator (VCO) with its associated ovens, crystals, and adjustment circuitry has been replaced by a commercial frequency synthesizer to extend the range of the system, improve the stability, and considerably reduce the complexity of operation. The phase-locked loops used for frequency shifting have been replaced by balanced mixers to eliminate acquisition control and reduce system complexity. Additional offset mixers and multipliers and their associated circuitry have been added to enable operation at either S-band or X-band.

Since the modifications, the reliability of the system has improved and operation has been simplified. During

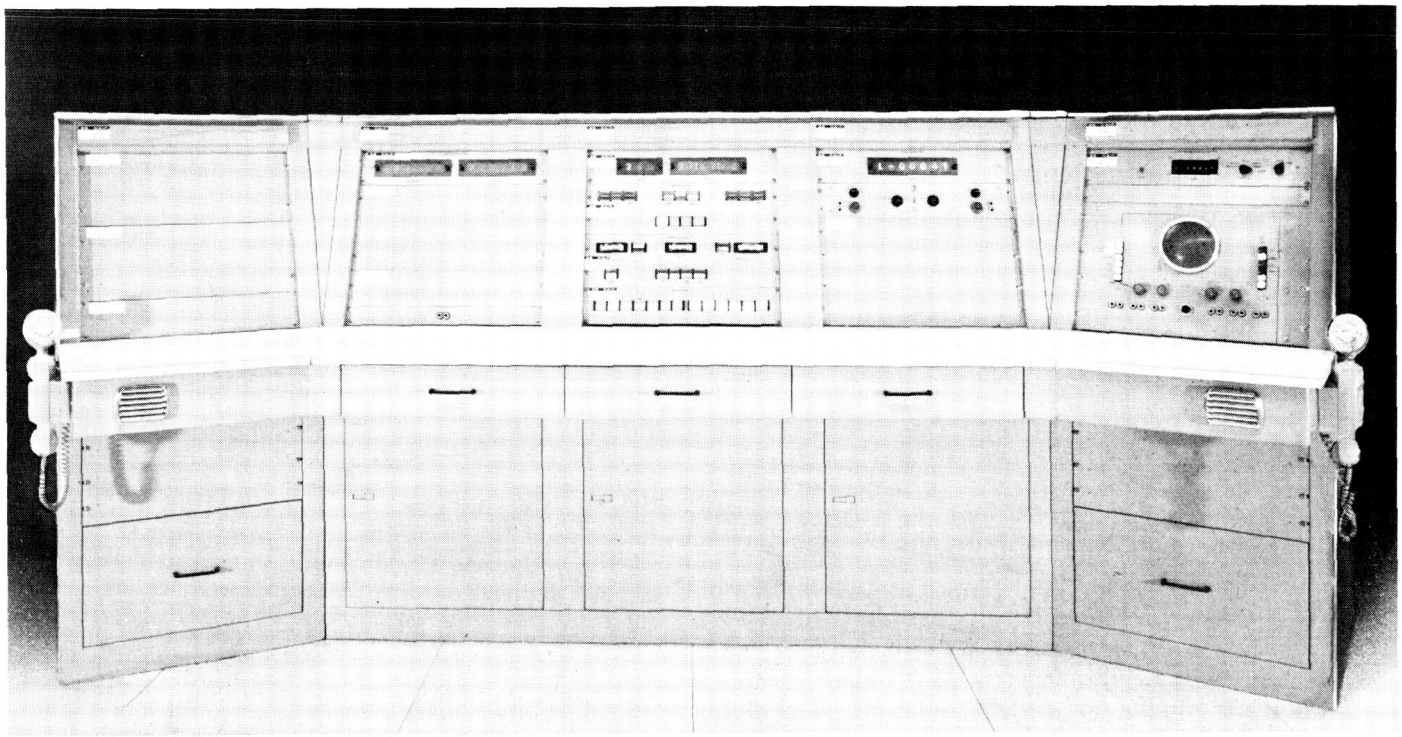

Fig. 3. Prototype station control and monitor console

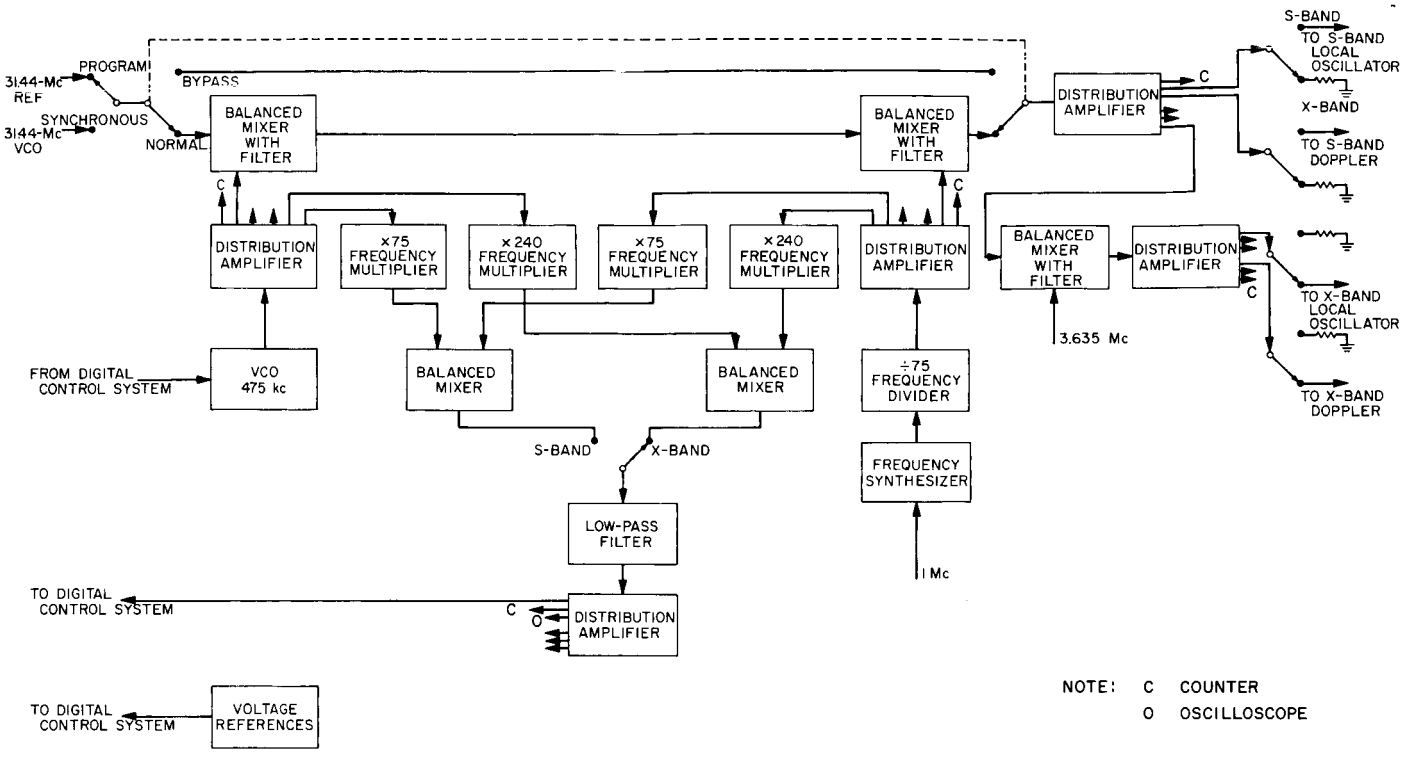


**Fig. 4. Programmed local oscillator**

recent X-band and S-band experiments, the system operated with only minor difficulties. The stability of the system while tracking doppler tapes is now $5 \times 10^{-11}$ rms at X-band (approximately 0.5 cps) and $13 \times 10^{-11}$ rms at S-band (approximately 0.3 cps). A large portion of the error at S-band is due to the $\pm 1$ count uncertainty in the doppler counter and roundoff errors in the doppler tapes; these errors are a much smaller percentage of the carrier frequency at X-band.

### 5. Digital Circuit Module Development

A prototype circuit has been developed for a 1-Mc clock oscillator module to be used as a basic source of the clock frequency in synchronous clocked logic systems. The circuit (Fig. 5) consists of a voltage-controlled crystal oscillator operating as part of a phase-locked loop. Operation of the oscillator can thus be either free-running or synchronized to an external 1-Mc reference standard without requiring any internal wiring changes when changing from one mode to the other. Tests indicate that the synchronizing or pull-in capability of the circuit to an external reference extends over a range of 200 cycles. The free-running oscillator sensitivity to power supply voltage variations of $\pm 10\%$ is less than $\pm 2$ cycles.

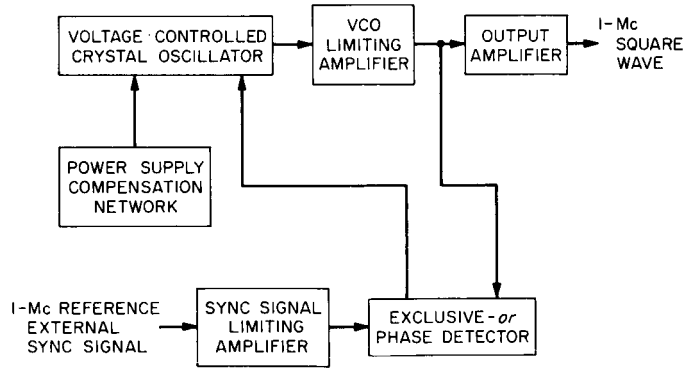


**Fig. 5. Clock oscillator circuit**

## D. Advanced Antenna System

### 1. Elevation Bearing Assemblies

Two elevation bearing assemblies have been delivered to the Mars Station. These two assemblies mounted atop the alidade support the tipping parts of the antenna

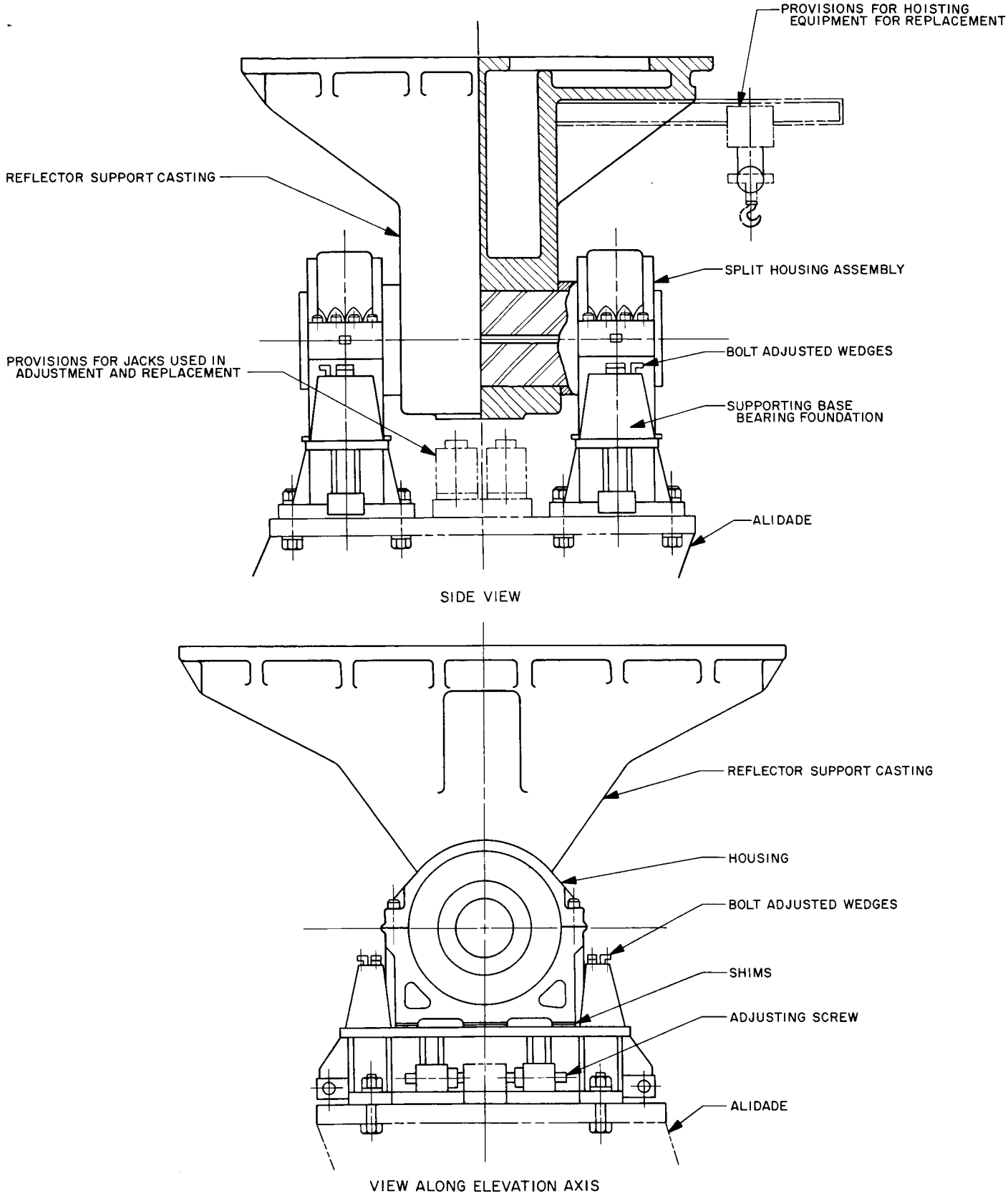


**Fig. 6. Elevation bearing assembly**

structure. Each bearing assembly consists of two split housings, support bases, two self-aligning spherical roller bearings, a stub shaft, a reflector support casting, and associated shaft seals and alignment and adjustment components (Fig. 6). The two bearings mount on each end of the shaft pressed into the reflector support casting. The shaft and reflector support casting, in combination, form the elevation rotating connection for the reflector and backup structure.

### 2. *Elevation Wheel and Primary Reflector Structures*

The elevation wheel structure supports the primary reflector structure, which consists of rib trusses radiating from a center hub. A tie truss supports the elevation wheel and the primary reflector center hub and is structurally integrated with the primary reflector structure. The center hub supports the feed cone and houses the optical instrument for monitoring the reflector surface.

System integration studies subdivided the rms design values of half the RF path length errors into design goals for various error sources: gravity, wind, thermal differentials, fabrication, field setting, and safety factor. The elevation wheel and primary reflector structures were assigned a 0.065-in.-rms design goal for gravity loading. Design calculations yielded 0.068 in. rms for gravity loading with the antenna at zenith and panels at 45 deg, and 0.064 in. rms for gravity loading with the antenna at horizon and panels at 45 deg. A balanced design was achieved, as is shown by the nearly equal rms values for perpendicular gravity conditions. The rms results were shown to be optimum.

# V. Space Flight Operations Facility

## A. Introduction

The Space Flight Operations Facility (SFOF), located in a three-story building at JPL, utilizes operations control consoles, status and operations displays, computers, data-processing equipment for analysis of spacecraft performance and space science experiments, and communication facilities to control space flight operations. This control is accomplished by generating trajectories and orbits and command and control data from tracking and telemetry data received from the Deep Space Instrumentation Facility (DSIF) in near-real time. The SFOF also reduces the telemetry, tracking, command, and station performance data recorded by the DSIF into engineering and scientific information for analysis and use by the scientific experimenters and spacecraft engineers.

## B. Orbit-Determination Keyboard

A keyboard input device has been designed and implemented at JPL for use in the flight path analysis area of the SFOF. This device replaces the existing control panel/control logic configuration used in updating the orbit-determination display (a display containing rows and columns of remotely controlled digital information). The purpose of the display is to present orbital and miss parameter information when the spacecraft is in close proximity to the Earth immediately after launch and during other critical phases of the mission. The keyboard input device was required to shorten the time involved in updating the display, especially during early phases of a mission when orbital trajectories have short periods due to the spacecraft's relative closeness.

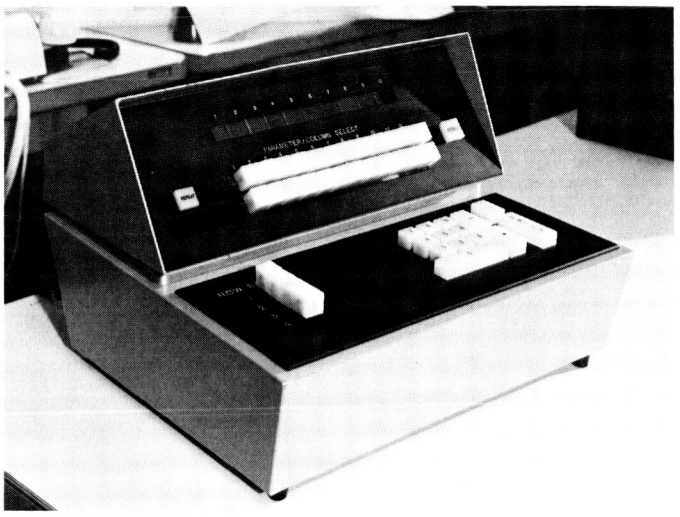

**Fig. 1. Keyboard remote control panel**

The new configuration consists of three units: a remote control panel (Fig. 1), a card-cage containing digital control logic, and a power supply. An updating operation will consist of selecting a column and row, "inserting" a selected array of ten digits into a shift register, and then entering these into the display proper. The new keyboard input device provides the same functions as the original system, with the additional capabilities of clearing the shift register in the event of an error and maintaining a given configuration of digital information in the shift register if two or more groups of ten digital data units are to be updated alike. The system has been tested and is fully operational. Evaluation of the system based on time-and-motion studies is favorable.

## C. High-Speed Data System

The high-speed data system (HSDS) is presently utilized in the transmission of real-time telemetry data from the DSIF stations to the SFOF. After performing data encoding, the HSDS transmitter phase-reversal-modulates an audio tone which is passed over high-quality voice transmission lines to the SFOF receiver. To be investigated are the errors which occur between the HSDS transmitter and receiver. Formerly, this task was often insurmountable because of the random nature of the digital signals which were passed. Fortunately, the operational HSDS design allows on-line performance monitoring of any type of random data.

The error-monitoring equipment consists of a counter, digital clock, and high-speed paper tape punch. In operation and on command from the counter, error count and Greenwich Mean Time are punched on the paper tape to provide a permanent record of line error characteristics. A computer program to reduce the error data reads the paper tape and provides outputs of error rate and performance evaluation. Thus, error data may be used to provide a basis for more efficient data-encoding schemes.

# SUPPORTING ACTIVITIES

# VI. Quality Assurance and Reliability

## A. Parts Reliability

***Mechanization of the reduction and analysis of parts reliability data.*** A mechanized data reduction system is being developed as an integral part of the JPL effort in electronic parts reliability. The primary objectives of this data system are:

(1) To validate reliability test results submitted by either parts manufacturers or screening contractors.

(2) To provide definition of the test results in terms of parameter distributions, parameter drift distributions, means, standard deviations, and other appropriate statistics.

(3) To provide means for management appraisal of screening effectiveness and technical trends such as lot-to-lot variability and vendor performance.

The system is being developed in three major phases corresponding to the three stated objectives. The first phase will accept raw data as received from the vendor, rigorously edit the data, and compare individual measurements with the limits prescribed in the detail part specifications. Parts failing to comply with the specifications will be listed in a lot performance tabulation by both failure category and part serial number. The tabulation will also indicate the total percentage of parts rejected and a breakdown of the total percentage by reject cause. In addition, an easily readable tabulation of all parameter measurements ordered by part serial number will be produced for retainment in a reference library.

The second phase of the system will employ the validated test data to compile statistics for each lot of parts received. To the degree allowed by the prescribed test sequence, the effect of separate test stresses will be defined in terms of actual parameter values, parameter drift, and percentage variation. For each lot, the output will consist of statistics such as means, standard deviations, parameter distributions, parameter drift distributions, and failure rates. Operations will also be performed to organize the data into lot groupings by part type for further analysis in the third phase.

The third phase will evaluate trends in the lot-to-lot performance of a given part type. Consideration will be given to factors such as reject rate versus time, the effectiveness of various test stresses, parameter variation, vendor performance, and the over-all part failure rate calculated from the data accumulated on all lots tested.

Also, comparisons of the over-all behavior of similar part types or of identical part types from different manufacturers can be made.

During November and December 1964, data requirements and definitions of the various data formats to be accepted by this system were brought together in the form of an engineering prerelease specification. The logic was completed for the first phase of the system, and computer programming of the first phase was initiated.

***Design appraisal of electronic parts.*** To complement the over-all parts reliability program at JPL, electronic parts are being subjected to a design appraisal. The primary objective of the design appraisal is to observe and identify physical relationships which indicate potential reliability problems, i.e., failure mechanisms in the part. This is accomplished through observation of such items as part design, construction, workmanship, and materials and a limited electrical investigation on a small number of devices. Hence, design appraisal is seen to be a method of prognosis, whereas qualification testing accompanied by failure analysis is a method of diagnosis. Except in the case of the very bad part, design appraisal cannot presently replace the conventional qualification/evaluation test. However, in most cases, design appraisal can assist in defining the most beneficial areas to investigate by tests.

The conceptual stage of the design appraisal effort was initiated in June 1964. At that time, a decision was made to consider the several major classes of parts sequentially rather than simultaneously. Nine semiconductor device types were selected for the initial set of appraisals. Laboratory work was completed on these devices in December, and reports on the effort are being prepared. Initial laboratory work is under way on twelve additional device types selected for appraisal. To establish broad guidelines for use in the appraisals, *Reliability Engineering Document No. 12* entitled "Semiconductor Design Appraisal Guide" was prepared. In relation to semiconductor appraisal, this document discusses foreign particles, bonding techniques, surfaces, hermeticity, thermal expansion, bulk defects, electrical behavior, and the package. A document of this type obviously cannot cover all aspects of the topics discussed and is primarily qualitative. Frequent revisions are anticipated due to new observations and advances in the state-of-the-art.

# VII. Environmental Testing Facilities

## A. Automatic Vacuum Failure Alarm System

One of the hazards of testing a spacecraft in a vacuum chamber results from an unexpected or uncontrolled increase in chamber pressure. Somewhere in the pressure range of 1 to $10^{-3}$ torr, a corona breakdown occurs between points with a high potential difference. This can and has resulted in damage to portions of the spacecraft under test when the chamber pressure unexpectedly passes through this range.

Experience has indicated that reliance upon manual cutoff of electrical power to critical circuits is usually inadequate to prevent damage, unless the pressure rise is quite slow (an improbable occurrence). The solution to the problem is to provide an automatic pressure-sensing system which de-energizes the spacecraft high-voltage power before the pressure increases to the danger level.

The pre-set actuation point for the shutdown system in the JPL 25-ft Space Simulator was established at $5 \times 10^{-4}$ torr. The pressure-measuring device selected for the system is an ionization gage. This, however, presents additional problems from the viewpoint of probable instrument failure as compared to the probability of a vacuum system failure. For this reason, three ionization gages are used in a circuit which requires the simultaneous measurement of a pressure above the prescribed limit. A block diagram of the system is presented in Fig. 1.

Since it is desired to limit the shutdown of the spacecraft power to a failure of the vacuum system, an AC relay, K4, connected across the 115-v power to the instruments prevents a shutdown due to console power failure.

Each Varian Associates ionization-gage control unit has a built-in alarm circuit which will actuate a relay contact at some pre-set pressure level. These relays, designated K1, K2, and K3, are set to actuate at $5 \times 10^{-4}$ torr. A normally closed contact is used to provide a system which requires the instrument to be operating and sensing a satisfactory pressure (i.e., less than $5 \times 10^{-4}$ torr) in order to open the relay contact. If a particular Varian Associates ionization-gage system fails, it can be taken out of the circuit by turning its power off.

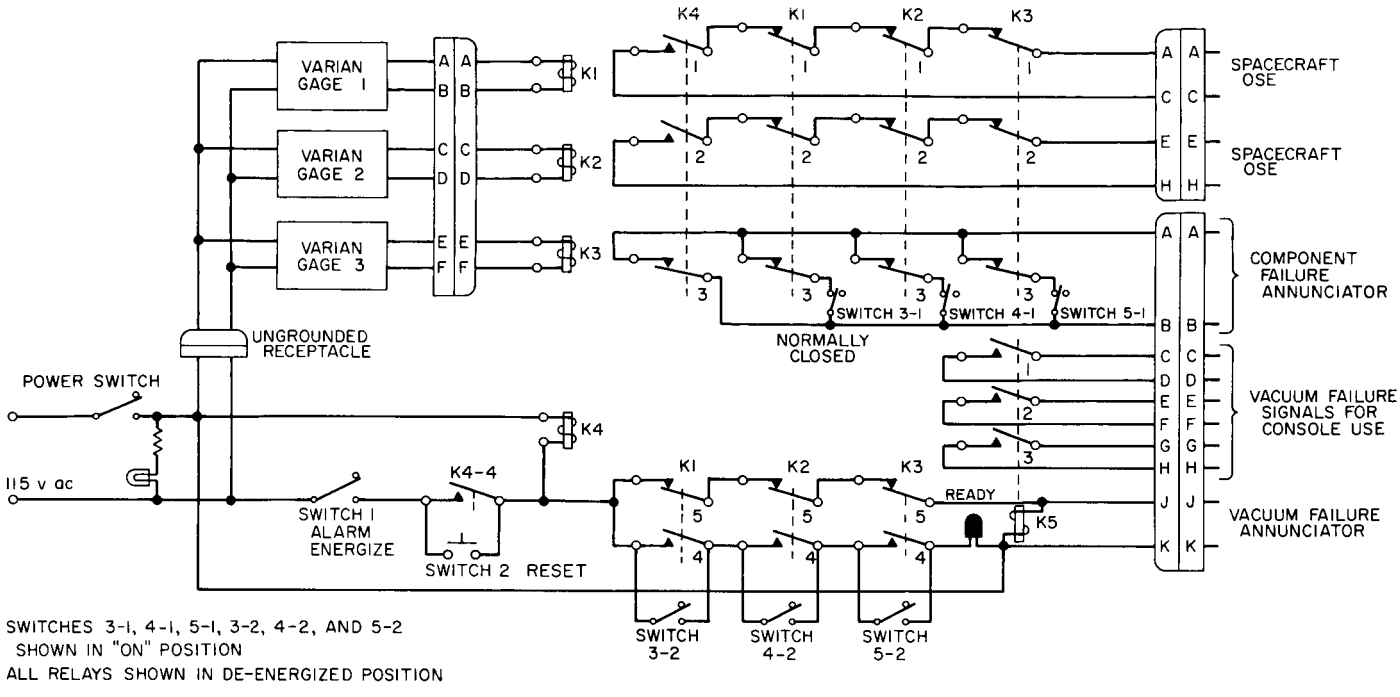


**Fig. 1. Automatic vacuum failure alarm system**

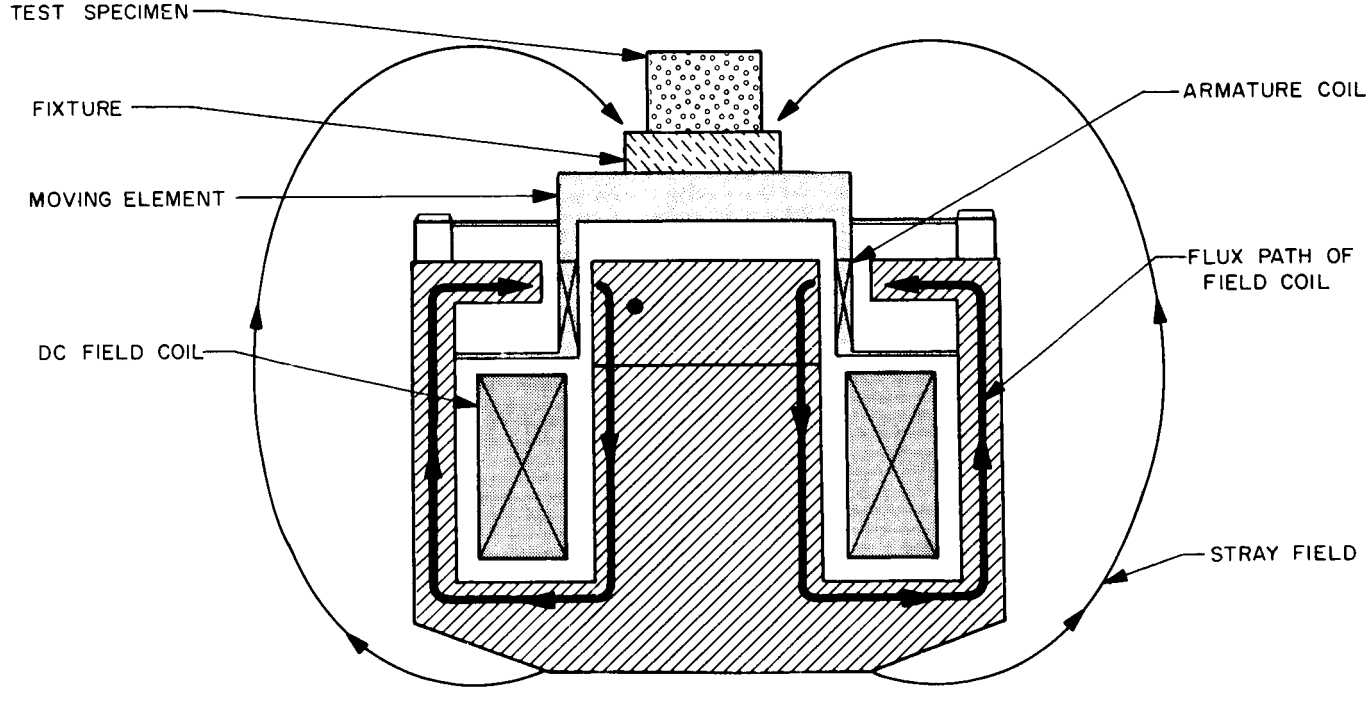


**Fig. 2. Simplified cross-section of a typical gap-end vibration exciter showing stray magnetic fields**

## B. Magnetic Shield for Use in Vibration Testing

*Minimizing stray magnetic fields in the electromagnetic vibration exciter.* Proper operation of spacecraft instruments (such as the *Mariner C* magnetometer and ion chamber) requires a maximum residual magnetic field of 5 $\gamma$, measured at a distance of 3 ft from the components. This requirement was impossible to achieve after the components had been exposed to the magnetic environment of any of JPL's operating electromagnetic vibration exciters due to stray DC magnetic fields produced by the exciters. The exciter fields are shown in Fig. 2, which is a cut-away view of a typical gap-end vibration exciter. The heavy arrows indicate the magnetic fields required for operation of the equipment; the light arrows indicate the stray magnetic fields which contaminate the component under test. Fig. 3 shows a vibration exciter in a horizontal position. A piece of cardboard with iron filings was placed at the top end of the exciter, and the pattern of the stray magnetic fields can easily be seen.

*Magnetic shield approach.* One way to solve the entire problem was to install an exciter of the new double-ended design in the environmental laboratory. However, the cost of the new equipment, plus the time required for delivery, installation, and testing, made this approach unacceptable. Therefore, the possibility of containing the stray magnetic fields by the use of a shield was investigated.

Several isolated instances were found where the stray fields had been minimized by enclosing the entire vibration exciter in a boxlike structure. There were several disadvantages to this approach: the structure was cumbersome; it required the use of an external exciter cooling

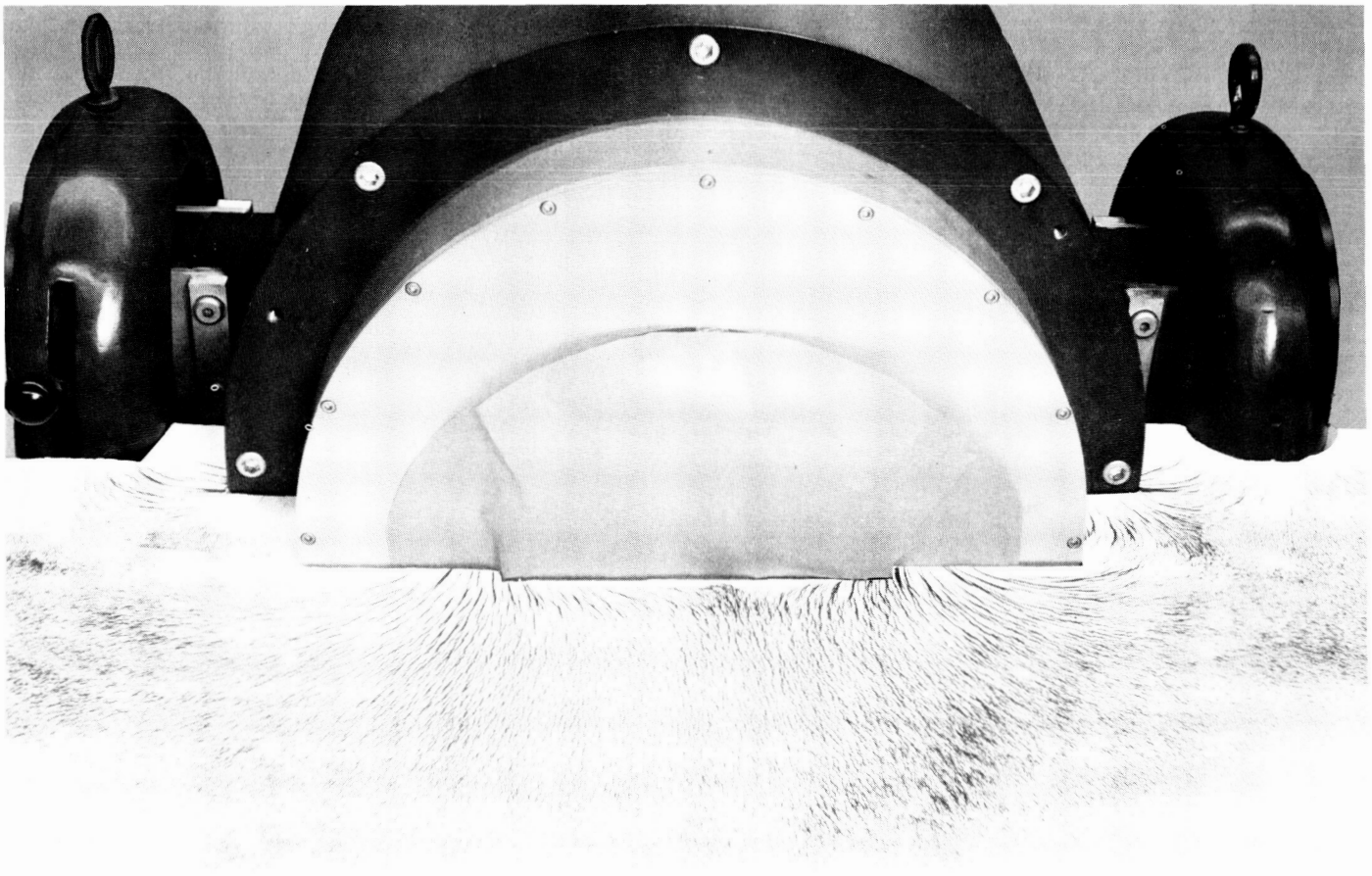

Fig. 3. Iron-filing demonstration of stray magnetic fields

system, an overhead hoist, and provisions for access to the unit under test; construction and installation of the device was time-consuming; the use of safety interlocks was required; testing and monitoring called for technically acute personnel; and the device was relatively expensive.

A much simpler shielding device was developed and proved to be entirely successful. Completed in about 1 mo at one-fortieth the cost of a new exciter system, the device provides a bypass path, i.e., a parallel magnetic diversion for the magnetic fields of the vibration exciter, at a safe distance from the component under test. The MB (Mettler Bros. Manufacturing Co.) Model C-70 vibration exciter was considered best suited to the adaptation of the device: its table-top magnetic field was lower than those of the other exciters, and it had an additional 2000-lb(f) output capability. With the shield installed, the table-top stray magnetic field dropped from 15 to 0.70 $\pm$ 0.40 gauss. (Measurements were taken using a field current of 11.3 amp and a degaussing current of 1.55 amp.)

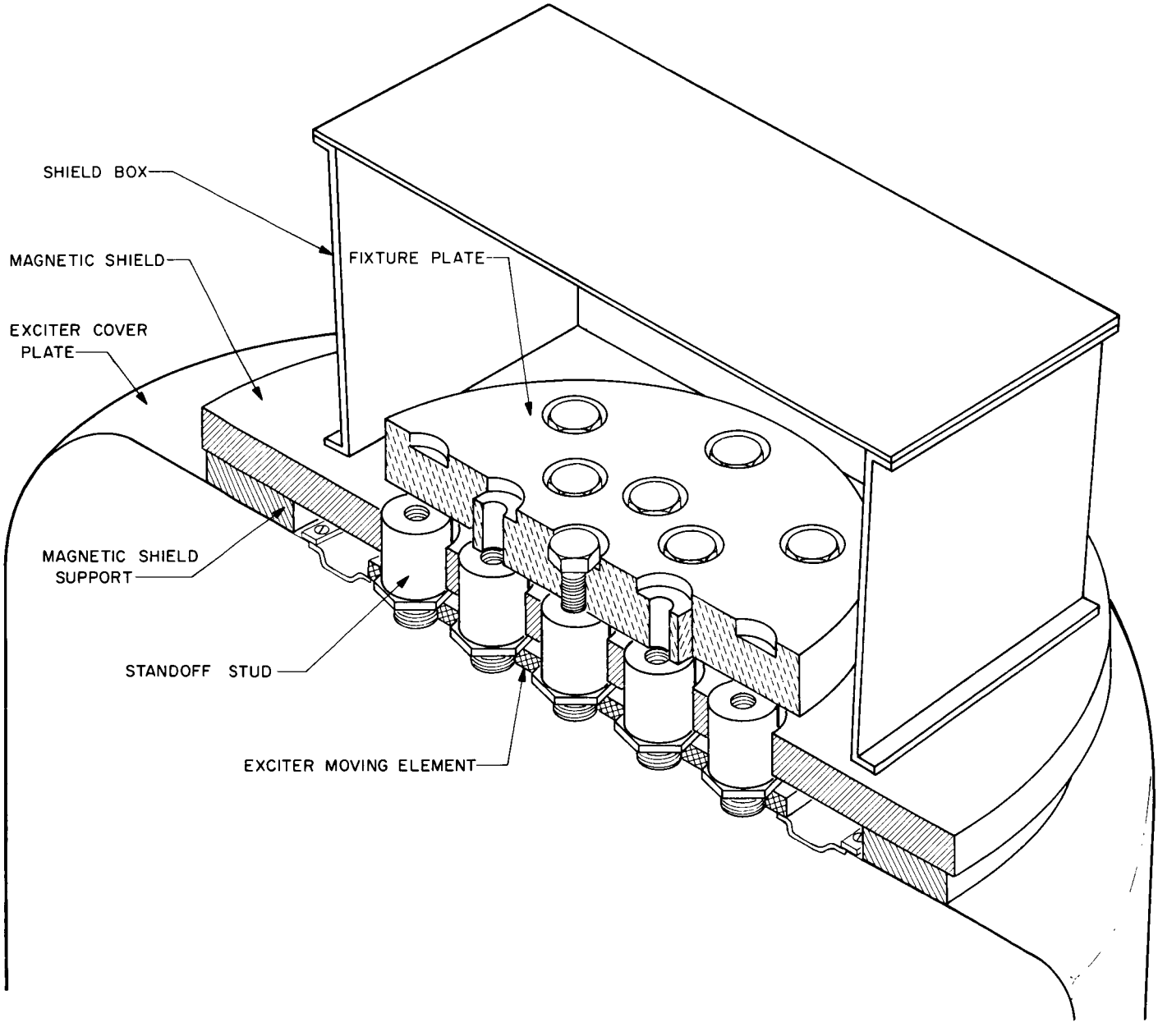


**Fig. 4. Magnetic shield installation on MB Model C-70 vibration exciter**

*Description of magnetic shield.* Fig. 4 shows the components of the magnetic shield installation. The shield itself is a round 34.5-in. D plate constructed of bonded Netic and Co-Netic layers (thin foils manufactured by Magnetic Shield Div., Perfection Mica Co.). The shield rests on a ⅝-in.-thick support ring which is attached to the exciter cover plate. The fixture plate (which holds the component under test) is attached to the top of the exciter by seventeen standoff studs. The standoff studs are inserted into the moving element of the exciter and protrude through holes drilled in the magnetic shield. The standoff studs allow for the vertical motion of the exciter, which has a double amplitude of ½ in. The shield box, covering the component under test, is placed on top of the magnetic shield before the exciter field is turned on. The box has an open bottom and a hinged cover and is constructed of bonded Netic and Co-Netic layers.

## C. Spectral Measurements of Solar Beam

Eppley Laboratory, Inc., performed spectral measurements of the solar beam in the JPL 25-ft Space Simulator from October 19 to 27, 1964. The instrumentation which was used consisted of the Eppley Mark IV and V filter radiometers, a Jarrell-Ash Model 82-000 grating monochrometer, and a Perkin-Elmer Model 99 prism monochrometer. The latter two are shown in Fig. 5 during calibration with a National Bureau of Standards tungsten filament spectral radiation standard. During test this lamp was removed, and light from the space simulator was reflected 90 deg by a front-surfaced spherical mirror and passed through a 6-in. D quartz window in the personnel door of the space simulator. The Mark IV and V radiometers were mounted within the chamber and were remotely controlled from the consoles shown in Fig. 6. The Mark IV radiometer had 12 narrow-band filters selected for the spectrum presented by mercury–xenon compact arc lamps and was able to measure totally and spectrally, in 12 bands, the radiant energy present. The Mark V radiometer had two filter wheels of 12 filters each; these filters consisted of both broad-band and narrow-band types.

Preliminary data indicate little spectral change from previous measurements made by Eppley in January 1963. The spectrum approximates that obtained from a mercury–xenon lamp and will be reported in more detail following complete data reduction and analysis.

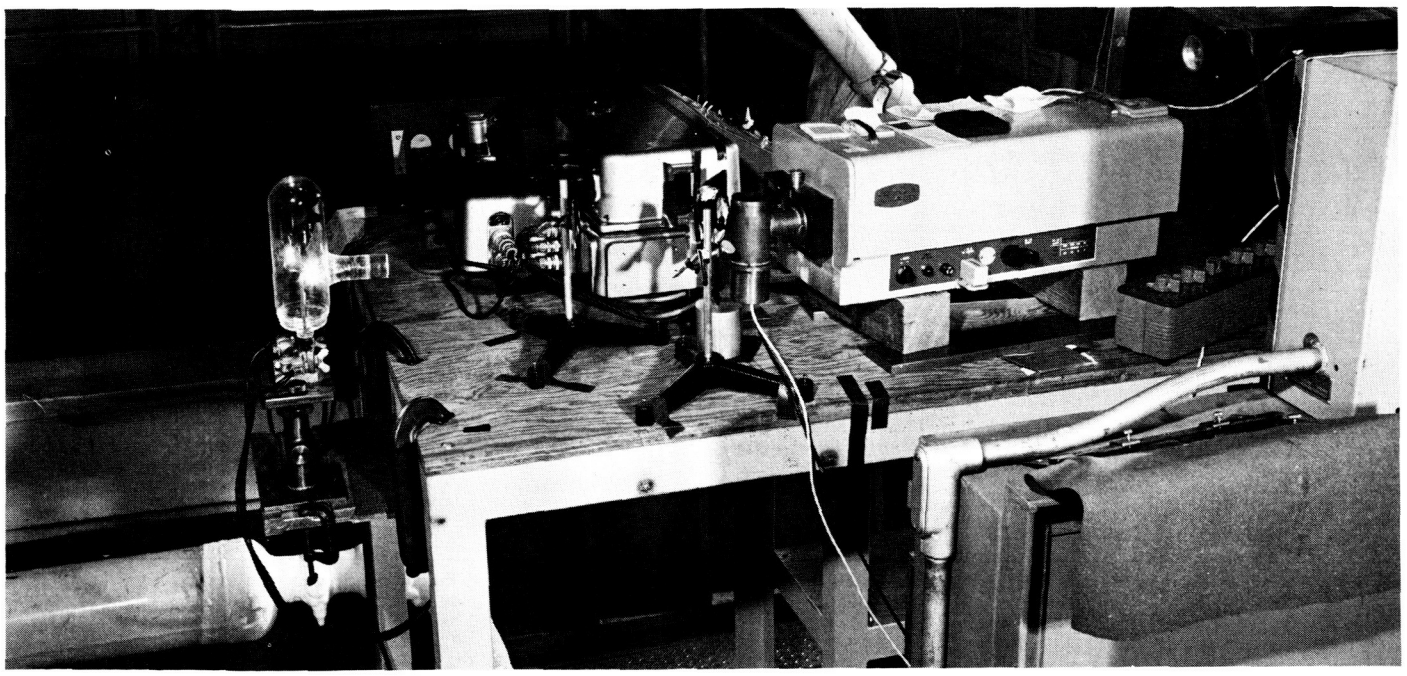

**Fig. 5. Calibration arrangement of Perkin-Elmer Model 99 and Jarrell-Ash Model 82-000 monochrometers**

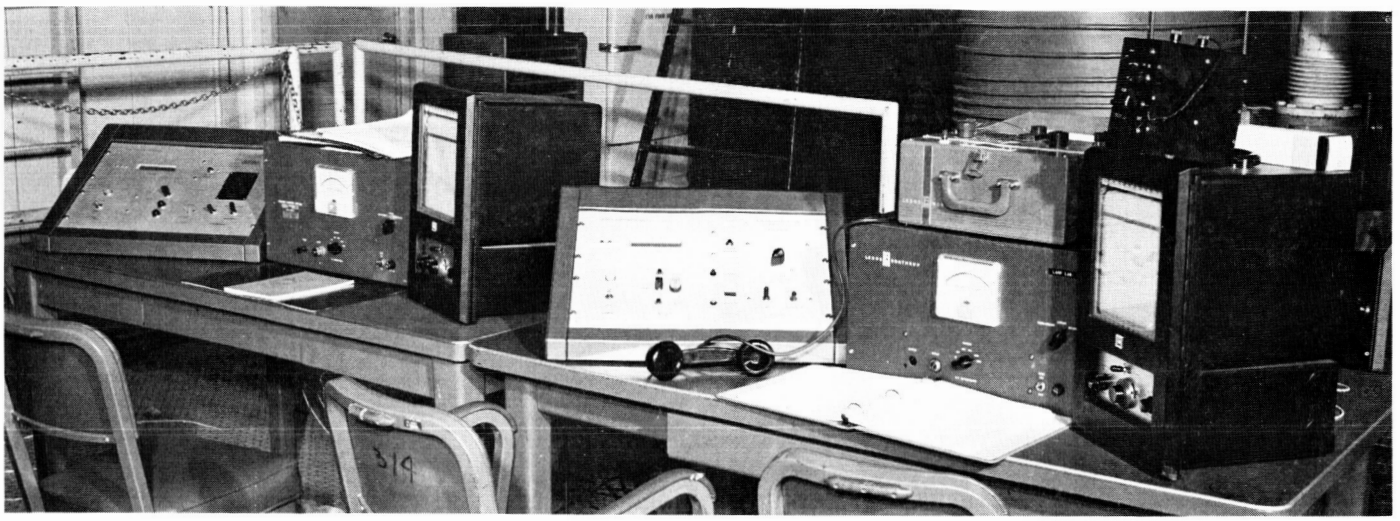

Fig. 6. Mark IV and V radiometer control consoles

SPACE SCIENCES

# VIII. Lunar and Planetary Instruments

## A. *Surveyor* Soil Mechanics Surface Sampler

***Introduction.*** The *Surveyor* soil mechanics surface sampler instrument consists of a motorized lazy-tongs mechanism equipped with an accelerometer and strain-gage sensors for measuring the forces developed during manipulation. The basic mechanism was originally designed by Hughes Aircraft Company (HAC) as a device for obtaining a sample of lunar surface soil and delivering it to a grinder for processing preparatory to analysis by other instruments. It was felt that with minor modifications plus suitable sensors, this surface sampler mechanism could be converted into an acceptable soil mechanics instrument. Developmental tests to date have verified this to the satisfaction of the principal investigator and the cognizant JPL personnel.

***Description.*** Fig. 1 shows the prototype unit, Serial X-4, mounted on the HAC Payload Systems Laboratory simulated spacecraft. The mechanism comprises five bays of 14-in. link members carrying a clam-shell scoop at the outboard end and supported at the base by a yoke motorized for motion in azimuth and elevation. Extension is accomplished by base springs and retraction by a motor-driven spool which carries the draw tape. A fourth motor opens and closes the scoop door.

Motion capabilities are 150 deg in azimuth, 70 deg in elevation, and 12 to 60 in. in extension. This permits the scoop to be deployed for picking, scraping, digging, or sample collecting from a sector of the lunar surface approximately 35 $ft^2$ in area—all of which is within the field of view of one or both of the survey TV cameras. The instrument dexterity will also permit it to clear an area of surface debris for observation by another analytical instrument, or to redeploy some other instrument, thus increasing its capabilities.

Each motor is reversible and may be commanded in coarse (2-sec) or fine (0.1-sec) increments. This permits a

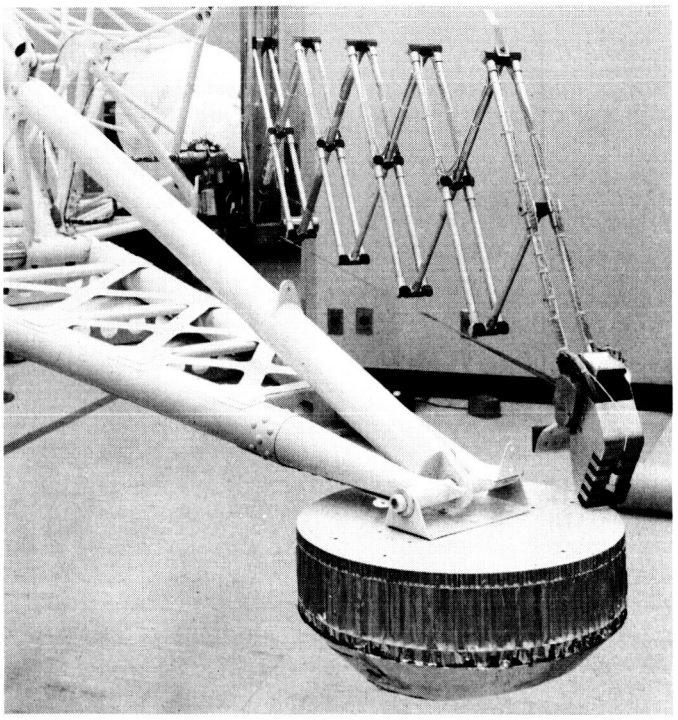

**Fig. 1. Prototype soil mechanics surface sampler X-4 mounted on HAC Payload Systems Laboratory simulated spacecraft**

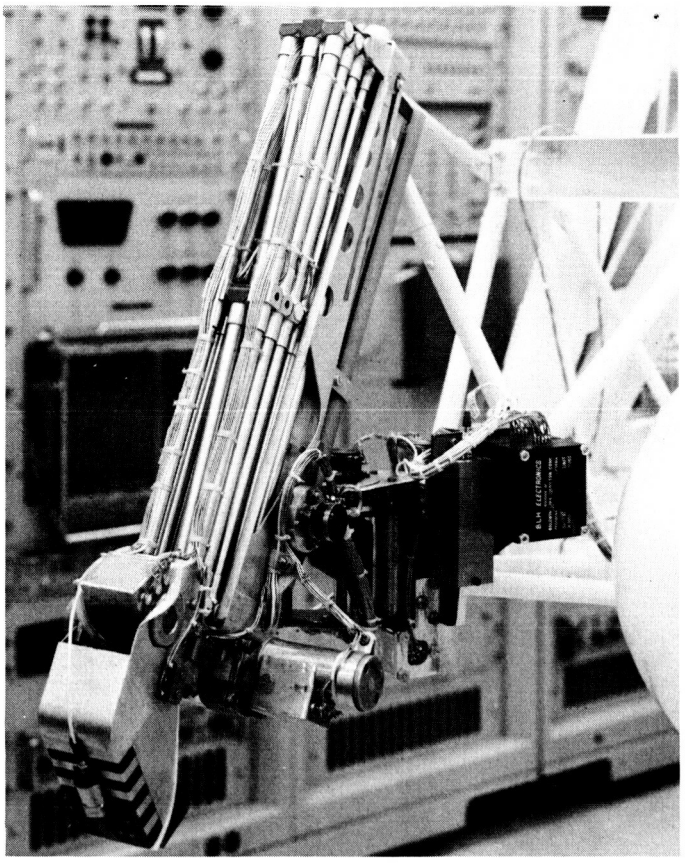

**Fig. 2. Stowed surface sampler showing the accelerometer, amplifiers, potentiometers, and microswitches**

wide degree of control of the scoop in mapping the local lunar surface or in repositioning the scoop for repeated digging or picking tests. Closing the scoop also changes the "footprint" configuration for bearing strength tests from a sharp tool–steel blade to a rectangular flat plate about 1 by 2 in. The force capabilities of the motors are in excess of 1 lb each direction in azimuth, 1 lb in extension, 20 lb in retraction, and 3 lb up or down in elevation. The scoop door can develop a 7-lb crushing force at the lip.

***Transducers.*** Seven transducers are provided for measuring forces, acceleration, and position of the scoop tip. These are three precision, sector-type potentiometers for indicating extension, elevation, and azimuth position; a pair of microswitches for monitoring the scoop door position; two sets of bonded strain-gage bridges with separate power supplies and amplifiers for measuring forces; and a piezoelectric acceleration sensor with an associated charge sensitive amplifier for picking decelerations. The accelerometer, amplifiers, two potentiometers, and the microswitches may be seen in Fig. 2 along with the extension motor-gear assembly. Fig. 1 shows the elevation strain-gage bridge attached to the center root member of the linkage. The other strain-gage bridge is mounted on a small strain-multiplying cantilever beam at the base of the scoop. This is hidden from view, but is at the point where the draw tape attaches to the scoop.

***Operation.*** The experimental operation of this instrument is planned to include a series of scraping, picking, and pressing operations in addition to the surface mapping mentioned above. The principal investigator is having a soil "catalog" prepared which will show typical signatures for various types of loose and solid materials that may be encountered.

Relative hardness of solid materials and the approximate character of granular soils may be determined by picking at a given spot. This is accomplished by elevating the scoop and then releasing a solenoid-operated clutch integral with the elevation motor assembly. A combination of torsion spring and gravity then drives the scoop onto the lunar surface while the accelerometer

monitors the deceleration trace for 2 sec following release of the clutch. This signal and the output of the elevation potentiometer are transmitted to the Deep Space Instrumentation Facility as analogs from which the velocity at impact—as well as the character of the deceleration—may be determined.

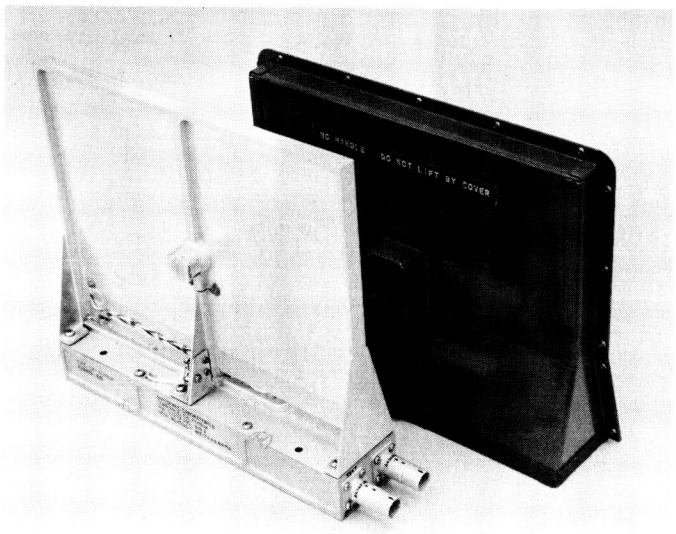

**Fig. 3. Micrometeorite ejecta detector sensor and protective cover**

A large degree of flexibility is provided for these deceleration tests. Elevation height may be varied from 0 to about 40 in. above the nominal lunar surface, the accelerometer amplifier may be switched for high or low gain (20:1), and the scoop may be used with the door opened or closed for a sharp edge or a large foot area. Measurable peak decelerations may thus be varied from approximately 0.1 to 20,000 Earth $g$.

The force measurements are essentially static, being read from a commutator along with the potentiometer, switch, and other outputs at the rate of 1/sec. Here, the scoop is positioned on the lunar surface and incremental motions of shear (draw tape) or bearing (downward elevation) are made. The gear trains are non-reversible from the output shafts so that the following force read is the one just developed. Skipping, jumping, or crunching may be variable and unpredictable so that a series of measurements will most likely have to be run before an intelligent estimate of the character of the lunar surface can be read.

## B. *Surveyor* Micrometeorite Ejecta Detection Experiment

The thermal analysis of the micrometeorite ejecta detector (MED) sensor assembly was completed. The


**Fig. 4. Type-approval-test micrometeorite ejecta detector sensor and electronics with the bench checkout equipment**

analysis indicated that painting of all sensor surfaces, except for the sensor thin films, with white inorganic paint is extremely important. Without the paint the maximum lunar day temperature of the sensor electronics was calculated to be 450°F, but with the white inorganic paint applied this temperature would be reduced to 213°F. The analysis also indicated that the 1-w sensor heater would extend the experiment operation time at lunar day terminator by only 6 hr.

Problems associated with applying the Hughes Aircraft Company (HAC) inorganic paint were avoided by utilizing the JPL organic/inorganic white paint and painting scheme. In addition, the upper limit of the operational temperature range of the sensor electronics had to be increased from 180 to 217°F, which required a slight redesign and retrofit of the prototype instruments.

Sensor covers to protect the sensor thin films and acoustic transducer from contact with foreign materials during testing and handling have been fabricated for each prototype sensor. The sensor covers also act to shield the acoustic transducer from acoustical noise. Fig. 3 shows a typical MED sensor and protective cover.

Fig. 4 shows the MED type-approval unit operating with the MED bench checkout equipment (BCE). The BCE is capable of simulating all the spacecraft commands to the experiment in addition to monitoring the instrument performance. The 19-bit data readout is automatically displayed in digital form and in the proper format every time the calibration or readout command is initiated.

***Micrometeorite ejecta detector auxiliary.*** In response to a JPL request, HAC has submitted an engineer-

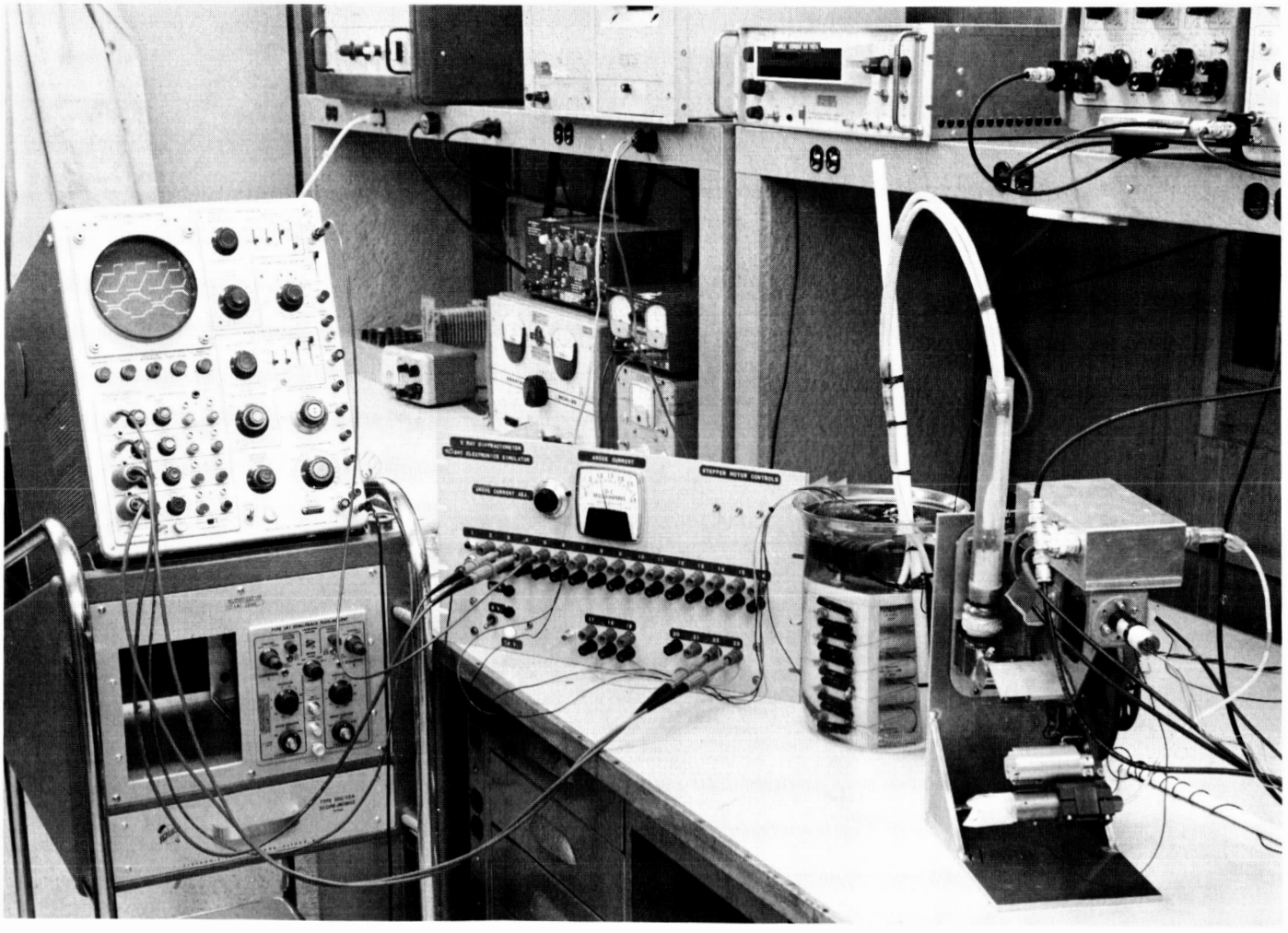

**Fig. 5. Diffractometer test setup**

ing change proposal which will provide current limiting for the experiment. This proposal provides for a redesign of the MED auxiliary 29-v-dc switch circuit to limit instrument current to less than 200 ma in case of a malfunction in the power circuits. The proposal also covered fusing of the 22-v heater circuit.

## C. Advanced *Surveyor* X-Ray Diffractometer

***Introduction.*** Philips Electronic Instruments produced the first approach to the design of an X-ray diffractometer for an on-site lunar-rock powder analysis. The latest prototype instrument (P-5) consists of three major packages: power supply, scan drive logic, and goniometer. High-voltage (25-kv) cables and connectors are required between the packages. The P-5 instrument has a total weight of approximately 25 lb, of which 15 lb is the goniometer weight and 9 lb is the power supply weight. The total volume is estimated to be approximately 1000 in.[3] The required continuous power is about 65 w, with a constant current of 2.2 amp and a transient current at turn-on of about 4 amp.

Based on the acceptable functional performance of the P-5 approach and the knowledge that the instrument design could be optimized, it was decided to proceed with a redesign of the diffractometer electronics. The primary objectives of the redesign effort are: (1) to reduce instrument weight and required power, (2) to unitize packaging, and (3) to improve reliability. The redesign is based on the use of integrated circuitry and an enclosed oil-immersed high-voltage power supply (i.e., no high-voltage cables or connectors).

***High-voltage (25-kv) power supply.*** The 25-kv power supply was redesigned and tested with all high-voltage components and connections operating in an oil bath. This technique eliminates all arcing. The test setup is shown in Fig. 5. The bottom two traces on the oscilloscope are the waveform across the high-voltage transformer primary. (Note the duty cycle and core collapse curve.) The anode current is shown to be 1 ma on the front panel meter.

Fig. 6 shows the high-voltage aquarium, a gallon beaker which contains the high-voltage transformer and rectifier–multiplier assembly. This beaker is filled with transformer oil. The two cables tied to the Teflon support rod lead to the X-ray tube. The method of attaching these cables to the X-ray tube for testing the feasibility of using oil as an insulator in the vicinity of a hot X-ray tube is shown in Fig. 7. The large shrink tubing contains the oil.

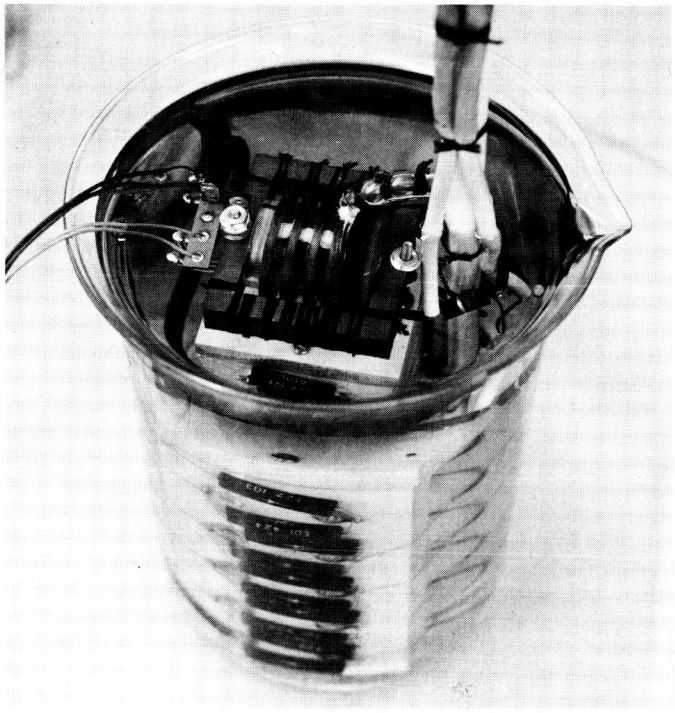

**Fig. 6. High-voltage aquarium**

The breadboarded electronics for the high-voltage power supply and motor drive system is shown in Fig. 8. A metal, hermetically sealed, oil-filled package has been designed to contain the supply. Fabrication of the high-voltage package will be completed during January 1965.

Power supply efficiency has been increased from 60 to 83%. The anode current is regulated over the temperature range of −50 to 100°C to 0.1% of 1 ma. This accuracy is also maintained over a power supply variation of ±5%. The current is regulated using pulse-width modulation techniques instead of the previous Class A method. Integrated circuits are used to mechanize the preamplifier, pulse-width modulator, and pre-driver.

***Power amplifier and anode current control loop.*** The output of the pulse duration modulator (PDM) is applied to two *and* gates along with an *on, off* function and a bi-phase drive (Fig. 9). Without the PDM, the output of the power amplifiers would be a 4-kc square

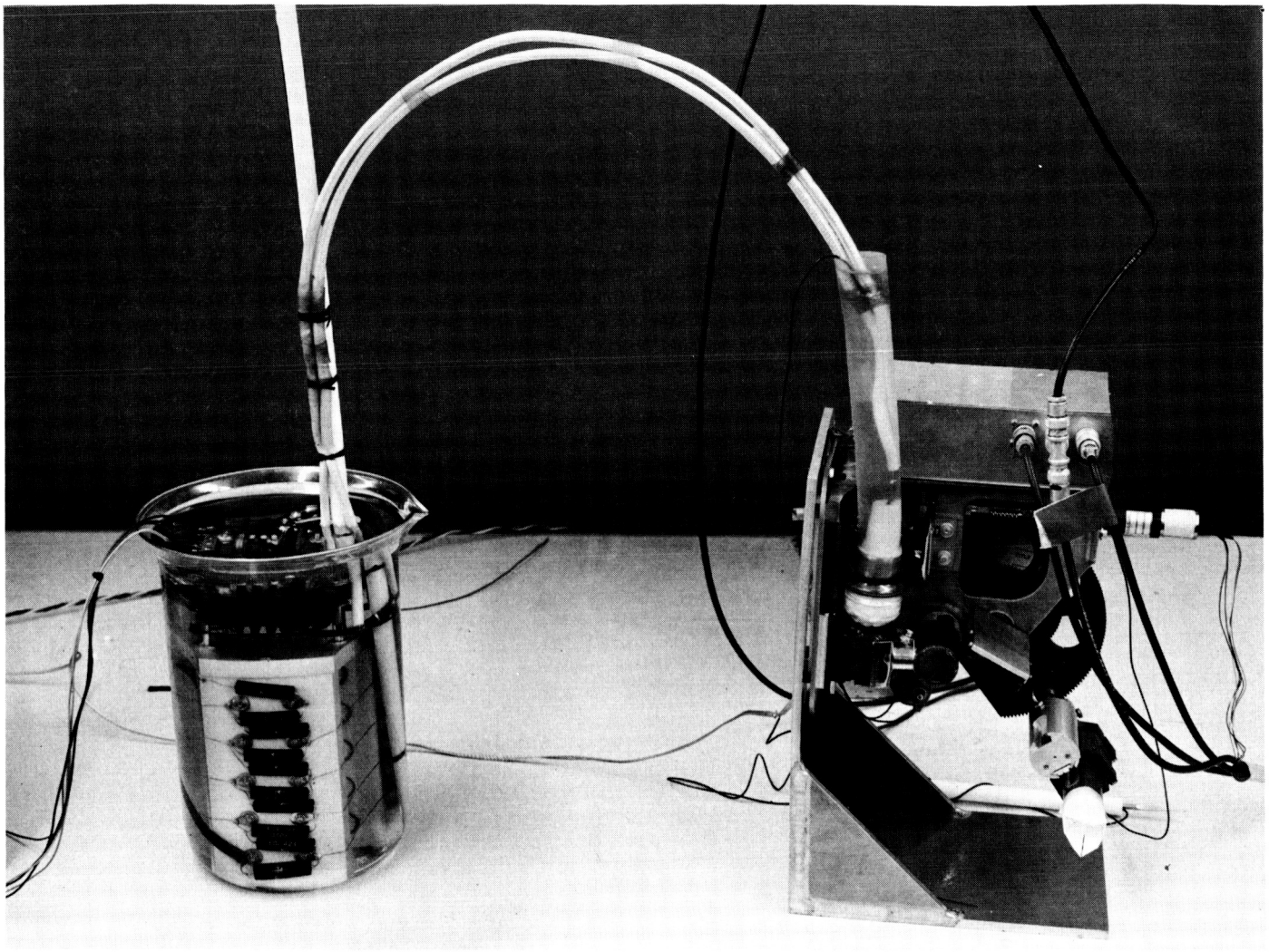

**Fig. 7. Goniometer and high-voltage aquarium**

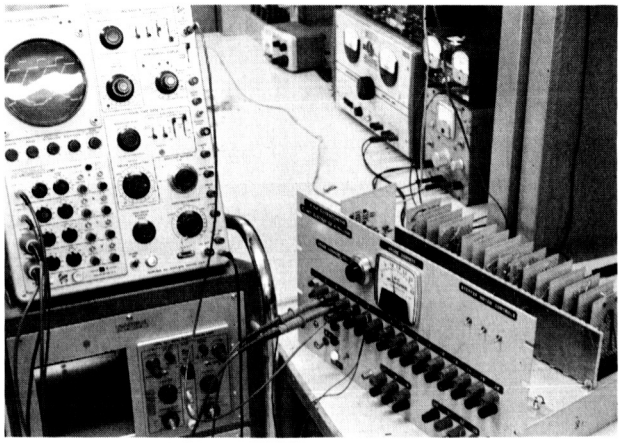

**Fig. 8. Flight electronics simulator**

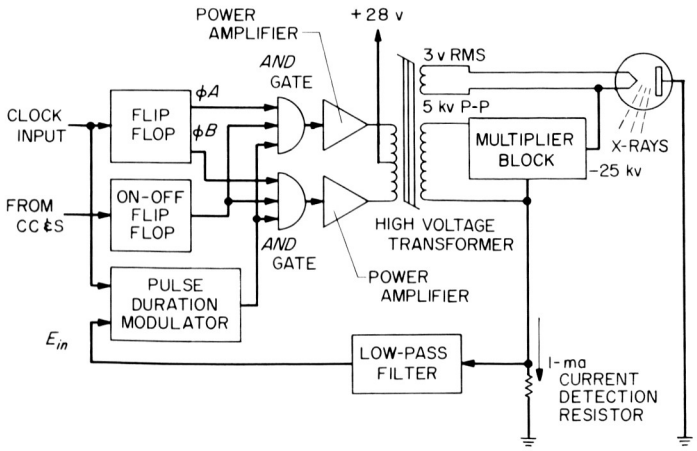


**Fig. 9. Power amplifier and anode current control loop block diagram**

wave driving the high-voltage transformer. As the filament of the X-ray tube heats up and 25 kv is applied, the anode current flows through a resistor, which in turn develops a voltage directly proportional to the anode current. The voltage across an 8.5-kΩ resistor is applied to the PDM, which then varies the duty cycle of the square wave across the transformer. The rms value of this square wave controls the filament temperature, thereby keeping the anode current constant at 1 ma through the action of the PDM. Since the multiplier block is essentially a peak-sensitive rectifier, the high voltage does not vary. In practice, though, it varies approximately 5% and in such a manner as to be self-regulated against line voltage changes. It can be seen in Fig. 10 that the anode current and anode voltage are essentially independent of supply voltage.

***Pulse duration modulator.*** The PDM makes use of Texas Instruments Incorporated Series 52 linear networks connected as shown in Fig. 11. The integrator generates a triangular wave which is used as a comparison ramp at the input of the comparator. Its amplitude is determined by the clock-input repetition rate and the integrator time constant. The preamplifier section compares the voltage developed across a precision resistor in series with the anode of the X-ray tube with a precision reference voltage.

The output of the comparator, operated open loop, is a square wave whose rising and falling edges are generated when the ramp voltage equals the output of the preamplifier and rises above or below it. Fig. 12 shows the equivalent PDM input offset drift as a function of temperature.

***Counter–scanner.*** The data-handling system for the X-ray diffractometer consists of a 13-bit ripple-through counter (Fig. 13) and a series of *and* gates. The counter is driven by the output of the pulse-height discriminator (PHD). The *and* gates are driven by a 4-bit counter, which counts at a rate determined by the clock countdown system (64 pps). The counter is allowed to accumulate the pulses from the PHD for 1 sec. The input is then inhibited, and the scanner converts the accumulated count into a 13-bit serial word with a sync word at the beginning (Fig. 14). At the end of the 250-msec scan period, the counter is reset to zero and the goniometer is advanced 0.01 deg. This process is repeated every 1.25 sec until the goniometer has completed its 83-deg scan. While the counter is counting, the scanner reads out the digital shaft encoder and transmits the goniometer angle as a serial word to an accuracy of 0.01 deg. This is also a 13-bit word with an identifying sync word at the beginning.

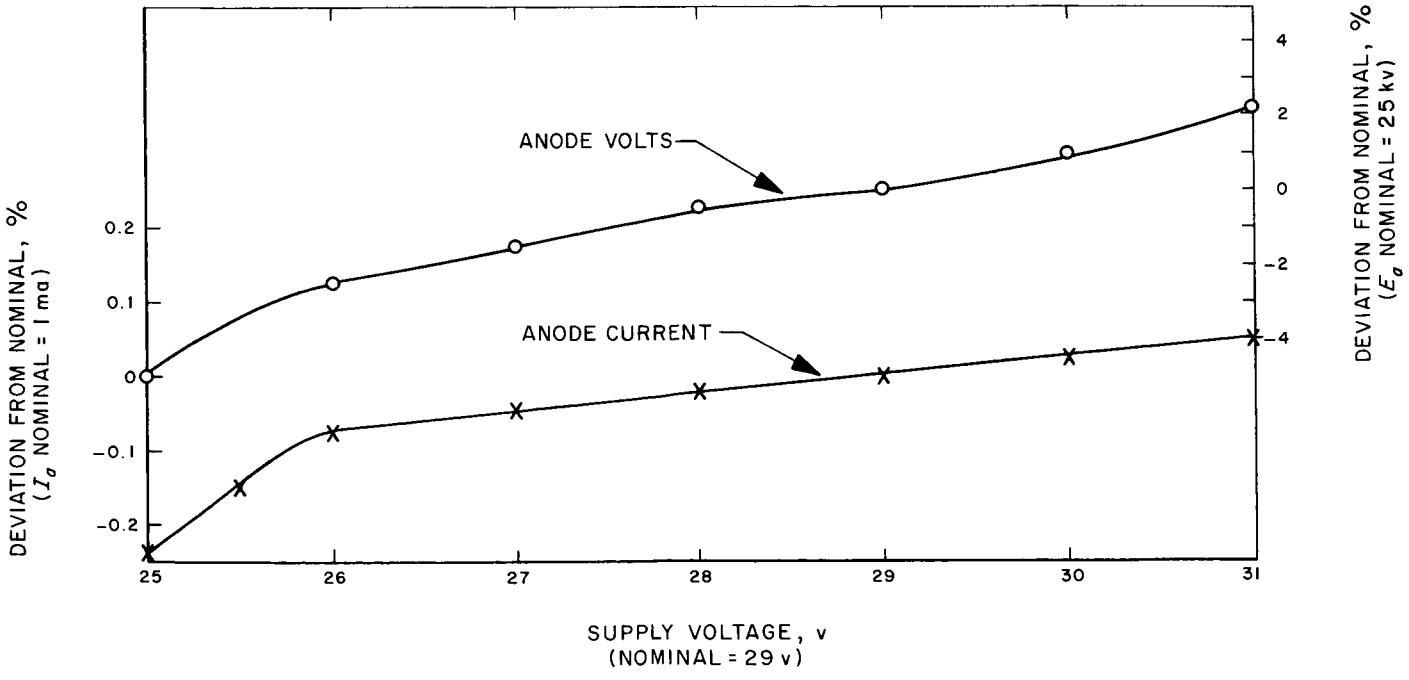


**Fig. 10. Variation of anode current and high voltage with supply voltage**

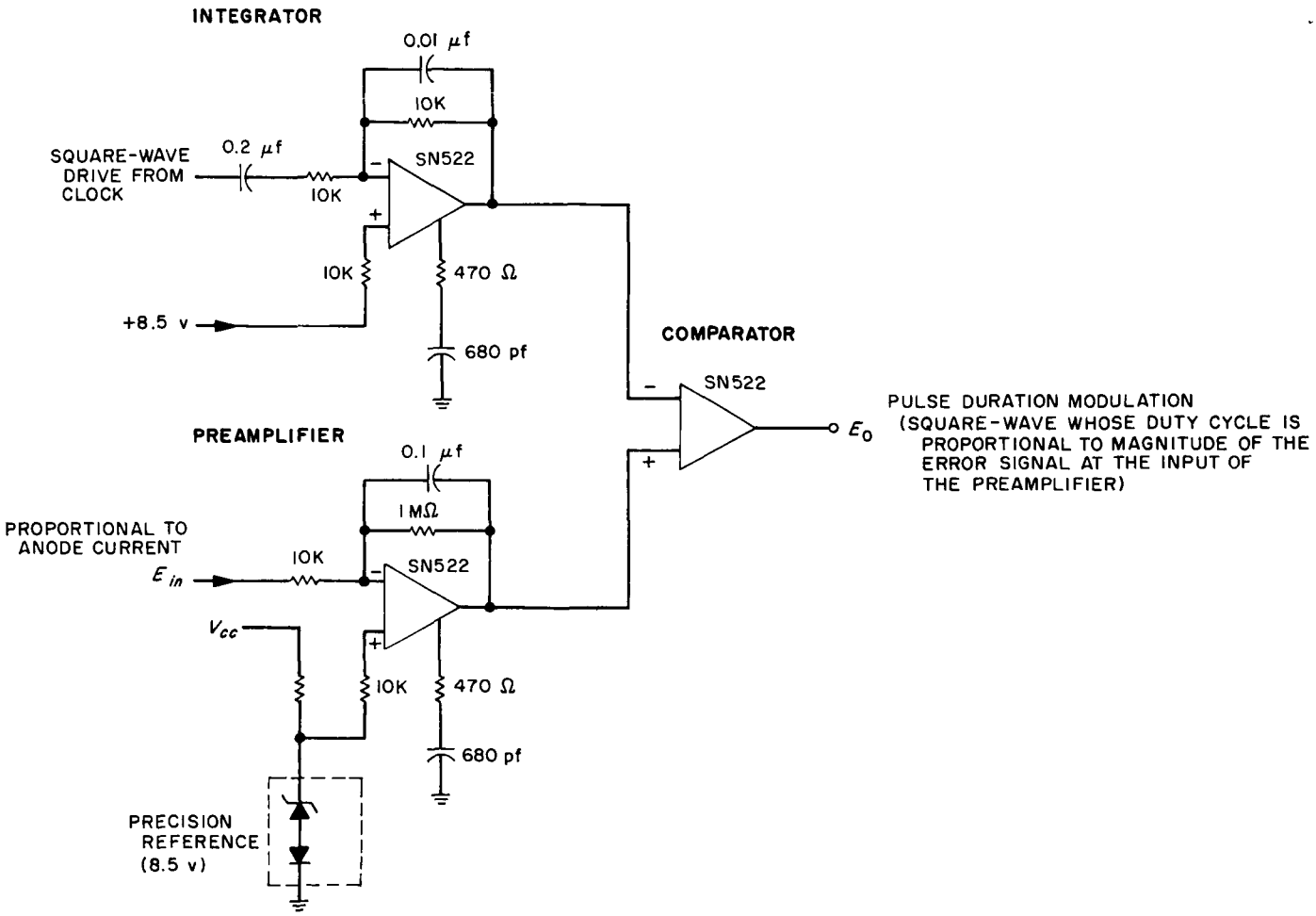


**Fig. 11. Pulse duration modulator block diagram**

*Pulse-height discriminator.* A PHD (Fig. 15) has been mechanized using two Texas Instruments linear networks and one Texas Instruments Series 51 gate network. The function of this device is to perform a pulse-height discrimination on the pulses appearing at the output of the proportional preamplifier. By setting the threshold control to eliminate noise and the window control to eliminate high-energy pulses, only those pulses generated by diffracted X-rays are allowed to pass through to the counter.

If Comparator 1 fires due to a pulse of amplitude greater than the setting of the threshold control, the pulse propagates through Gates 1 and 2 to the counter. If Comparators 1 and 2 fire due to a pulse of height greater than the window control setting, the pulse is prevented from passing through Gate 2. The settings of both the threshold and the window are remotely programmable. The variation of threshold and window voltages with temperature is shown in Fig. 16.

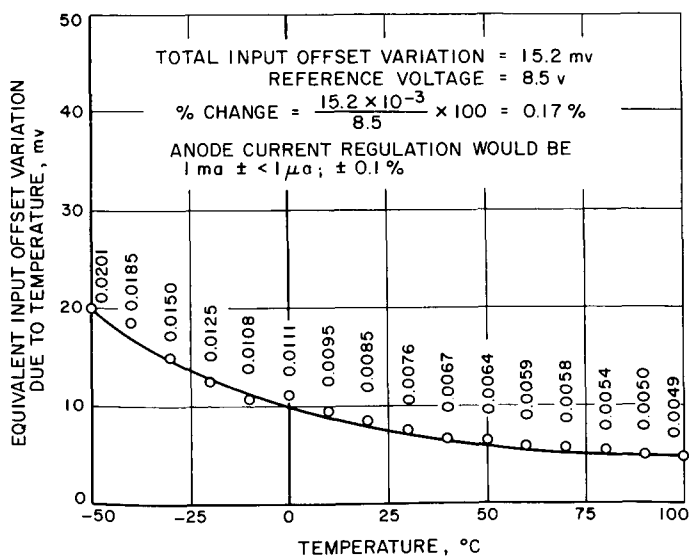


**Fig. 12. Results of temperature cycling of pulse duration modulator**

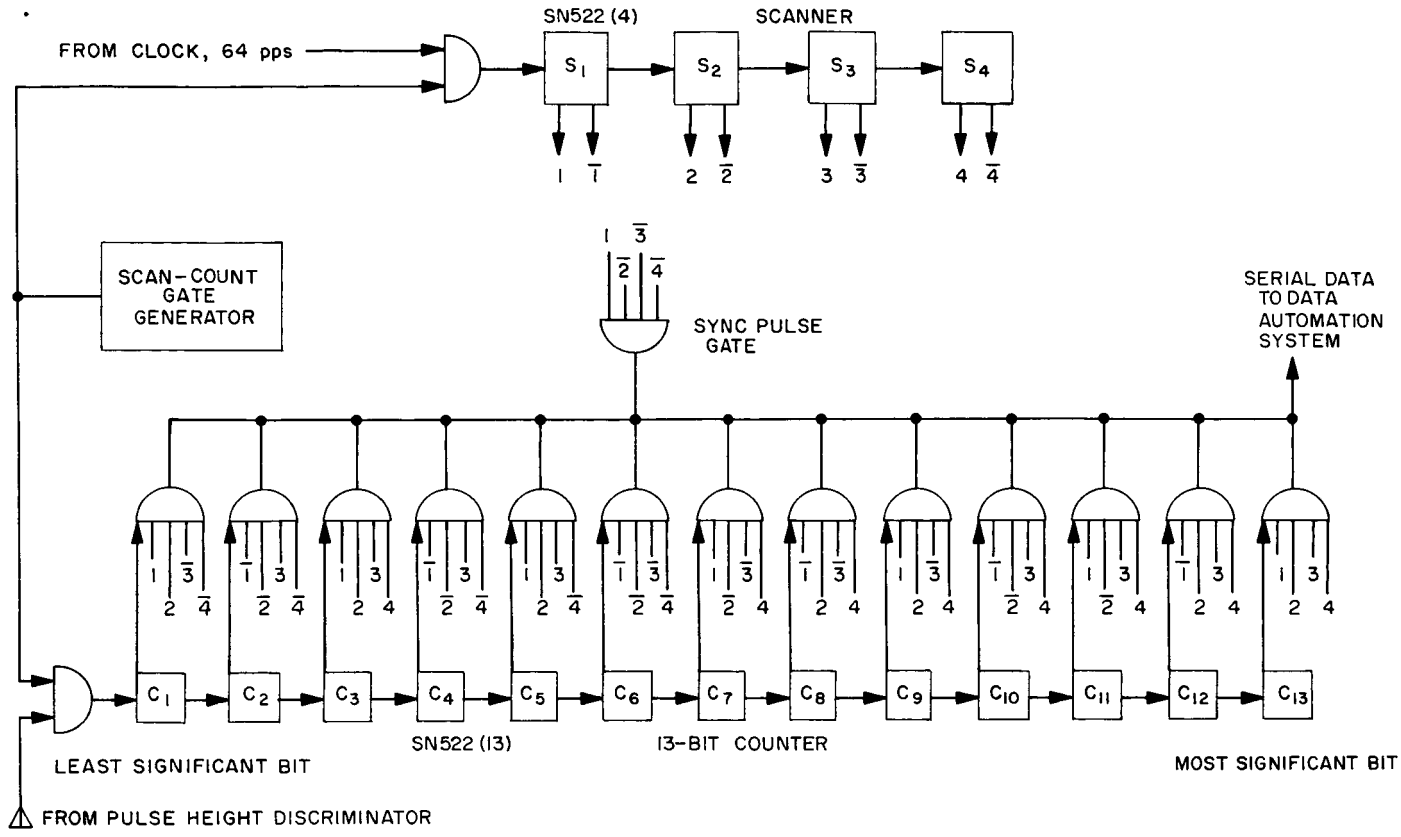


**Fig. 13. Counter–scanner block diagram**

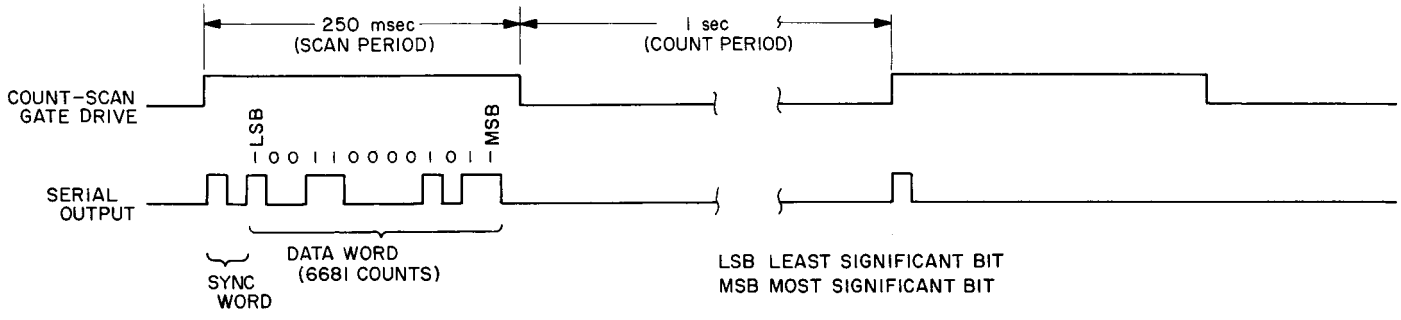


**Fig. 14. Counter–scanner timing diagram**

## D. Advanced *Surveyor* X-Ray Diffractometer–Sampler

The design and development work is continuing on the sub-surface sampling system to be used in conjunction with the lunar X-ray diffractometer. The sampler shall accomplish the following:

(1) Cutting (including drilling and pulverizing).

(2) Acquisition or collection of sample into extractor.

(3) Extraction and vertical transport of samples.

(4) Transfer and presentation of samples to diffractometer.

A sample extractor test rig (Fig. 17) has been designed and built to demonstrate the feasibility of a principle of sample extraction and vertical transport from a hole by vibration with minimum moving parts. A cross-sectional

view of the extractor is shown in Fig. 18. Tests are being conducted to: (1) determine and demonstrate the feasibility and effectiveness of the vibratory motion of a helical conveyor as a mode of extracting and vertically transporting samples from a lunar hole, and (2) gather data to evaluate design parameters and to indicate necessary changes in the design to produce an efficient and reliable sample extraction system.

To simulate lunar sample acquisition, these tests are being made with samples of basalt rubble, silica, sand, rutile, and mixtures of these in particle sizes ranging from 15 to 400 mesh and finer. The main parameters studied in the initial tests are:

(1) Drive speed (input rotational speed, rpm = vibration frequency, cycles/min).

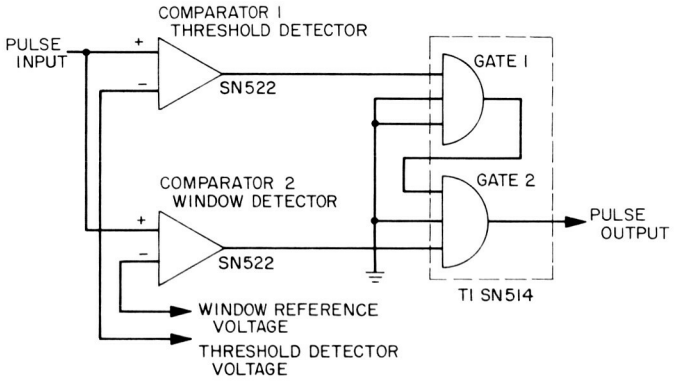


**Fig. 15. Pulse-height discriminator block diagram**

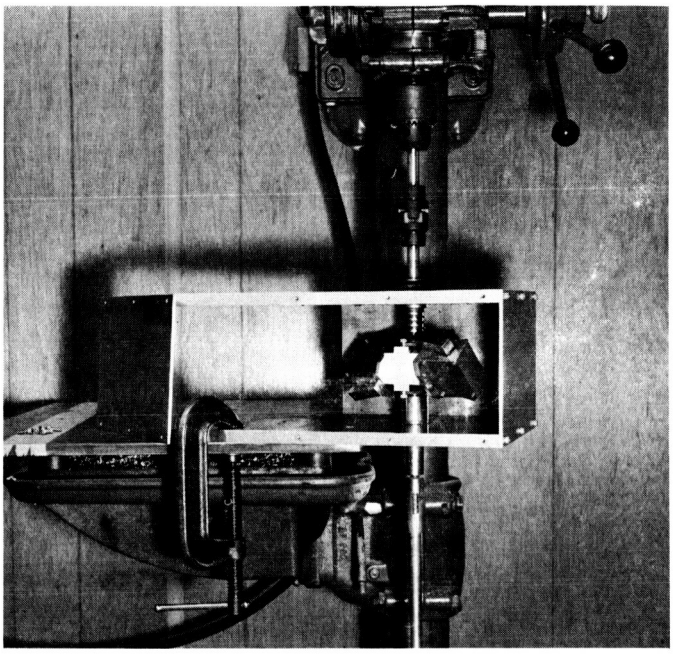

**Fig. 17. Sample extractor test rig**

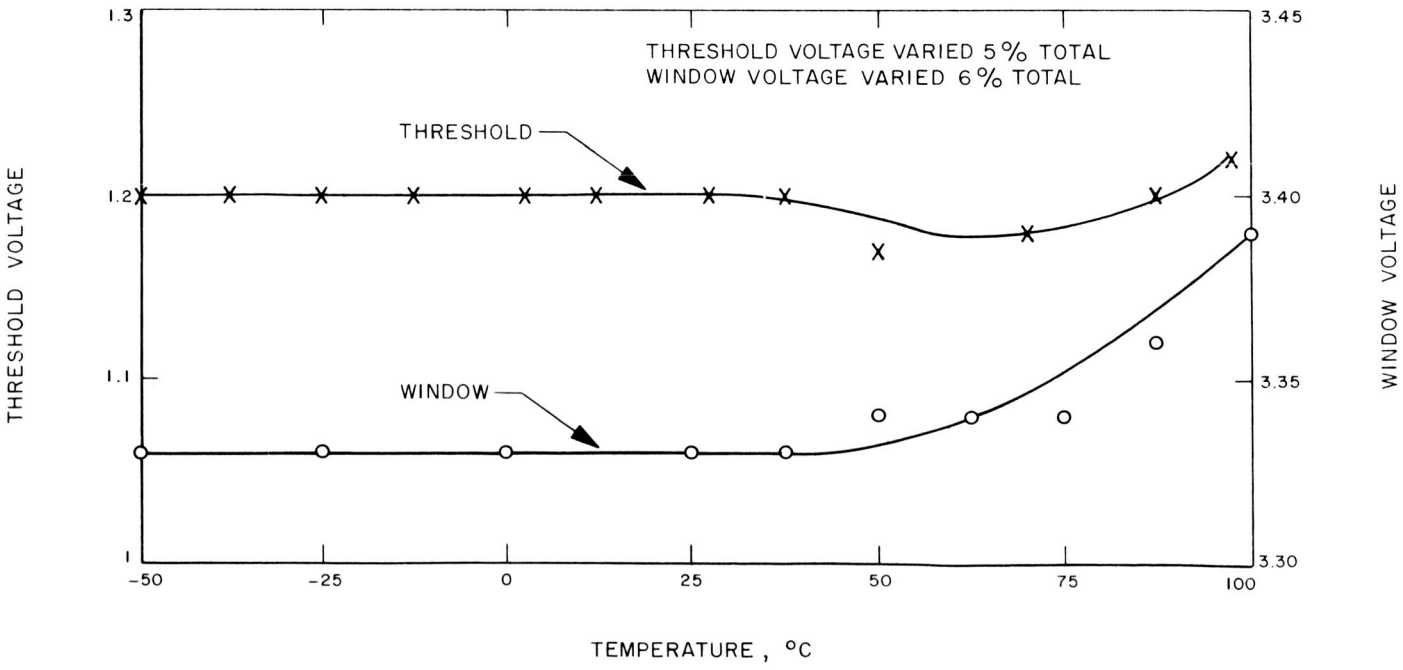


**Fig. 16. Variation of threshold and window voltages with temperature**

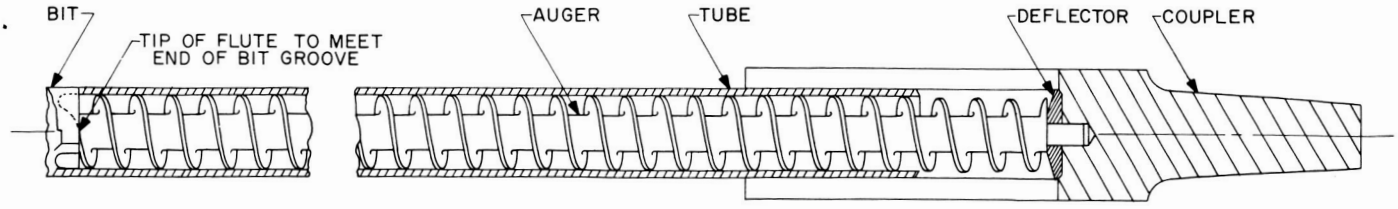


**Fig. 18. Cross-sectional view of extractor**

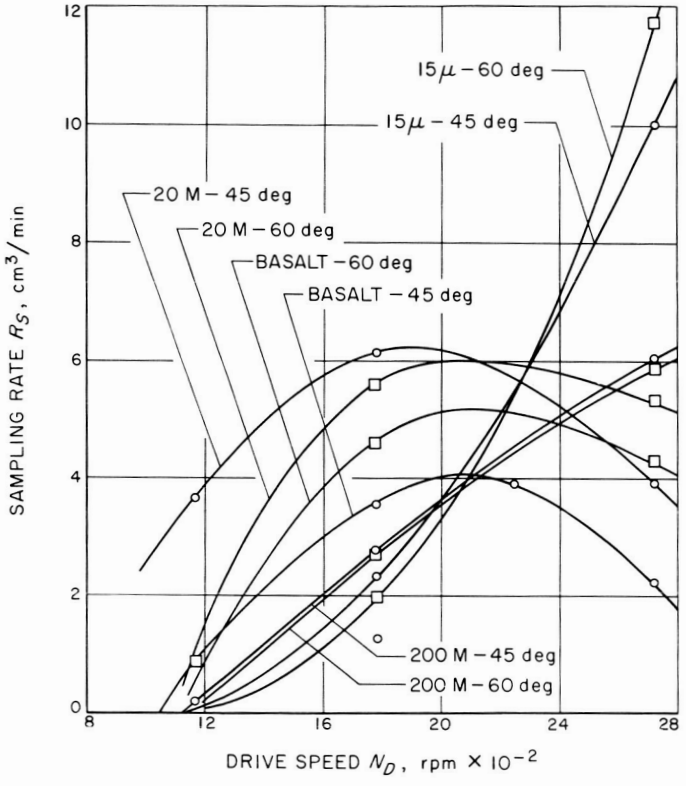


**Fig. 19. Sampling rate vs drive speed**

(2) Direction of drive forces. [The vibratory motion of the extractor bit, which occurs in both axial (linear) and rotary (torsional) directions, causes every point on the extractor bit to trace a helical path; the effective travel of each particle on the "helical conveyor" per vibration cycle is a function of (among other items) the relative amplitudes of the linear and torsional modes.]

(3) Sample particle size and density.

(4) Sampling rate ($cm^3$ of sample/min).

(5) Fractionation (separation, if any, of particles of different densities and/or sizes from a mixture during extraction).

(6) Angle of inclination of extractor axis to the local vertical.

Fig. 19 shows curves of sampling rate versus drive speed (vibration frequency) for various particle sizes and for drive angles of 45 and 60 deg. These tests have shown that the vibratory principle is feasible and that

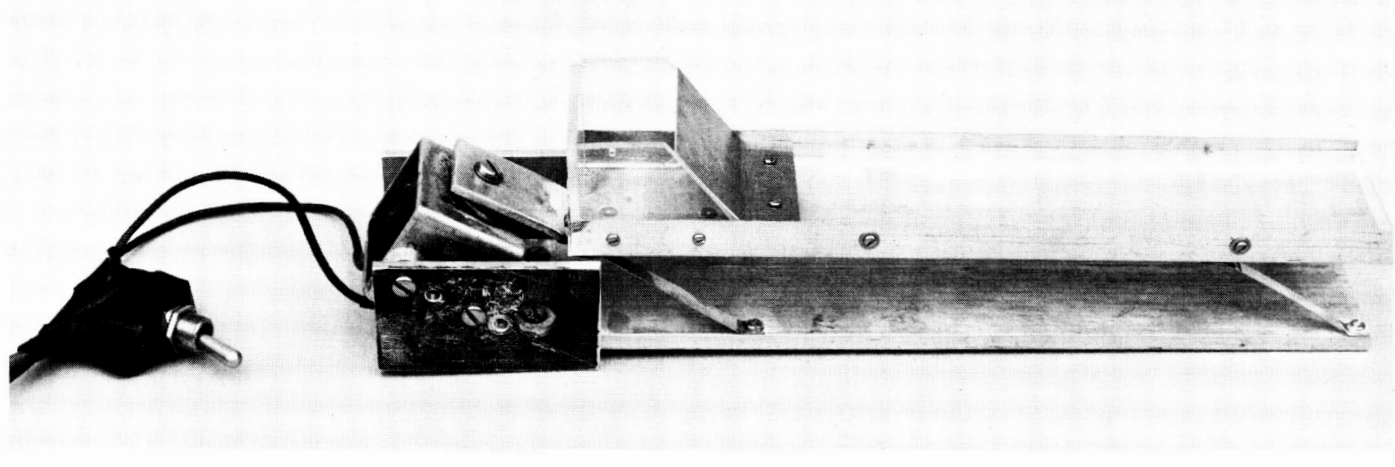

**Fig. 20. Vibrating tray test rig**

the extractor mechanism functions most effectively when the vibration frequency is approximately 2100 cycles/min and the drive force angle is about 60 deg. The extractor was run at a 15-deg inclination to the local vertical to simulate spacecraft tilt, and no changes in delivery rates and effectiveness were observed.

The endurance of the test rig was simultaneously tested during these tests. It has been in operation intermittently for a total accumulated running time of approximately 75 hr at various vibratory frequency levels and drive angles. Repeated tests made on certain samples have not indicated an apparent change in results; hence, no loss in effectiveness seems to have occurred.

Additional testing and evaluation of data and parameters necessary for design optimization will be made. Also, efforts will be made to study, design, develop, and test the mechanism for the transfer phase and the presentation of collected samples to the X-ray diffractometer. A simple test rig employing the principle of particle conveyance on a vibrating tray has been assembled (Fig. 20). This rig is primarily designed to investigate: (1) the use of a simple vibrating tray for the transfer and presentation phases of the system, considering all possible spacecraft orientations relative to the local axes; and (2) the problems of fractionation and contamination between samples of a continuous flow of powdered rock. The mechanism envisioned for this system is designed to receive the powdered rock from the extractor, transfer the powder to the sample station of the X-ray diffractometer, and support the sample and permit sample rotation by the goniometer drive mechanism.

The vibrating tray principle is feasible; however, its effectiveness and reliability is yet to be determined and demonstrated. A more complete assembly embodying this principle in addition to all the other required modes has been designed and will be built in the near future. A sample presentation system using discrete samples is also being developed.

In addition, the synchronization of the extracting motion with the motions required for cutting and sample presentation will be investigated. The complete X-ray diffraction instrument system shown in Fig. 21 will be used to demonstrate the feasibility of this integrated diffractometer sampler approach. The mechanism test rig designed to study the synchronization of the drilling, cutting, sample acquisition, and extraction phases has been assembled and will soon be ready for tests. The synchronous extractor drive assembly is shown in Fig. 22.

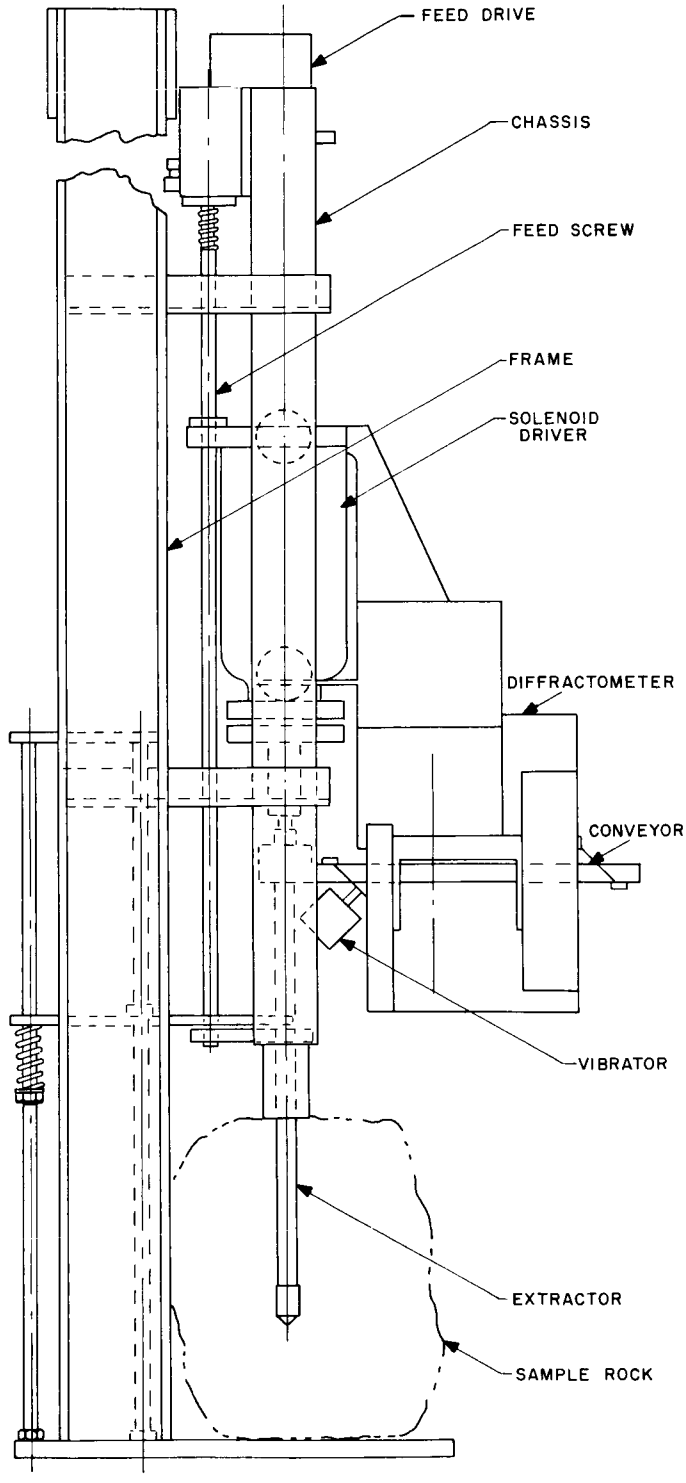


**Fig. 21. X-ray diffractometer sampler system (¼ scale)**

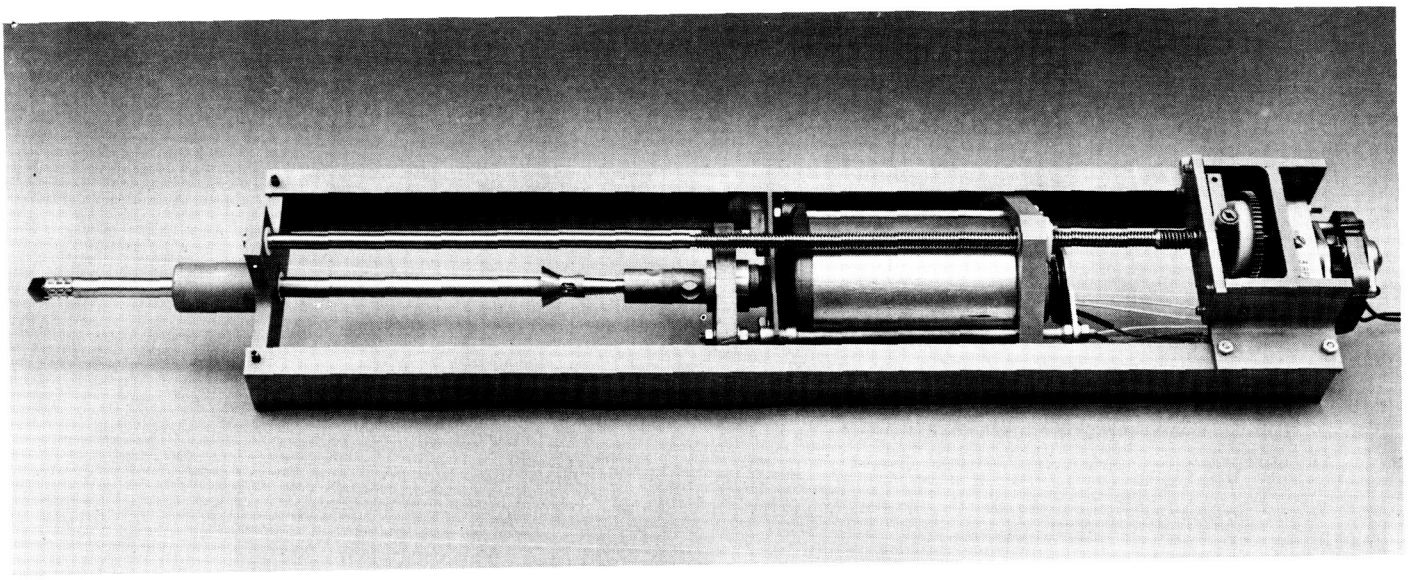

Fig. 22. Synchronous extractor drive assembly

# IX. Space Instruments

## A. Magnetic Shields to Support *Mariner C* Magnetometer Testing

This report describes two magnetic shields developed to support environmental and bench testing of the *Mariner C* magnetometer. Both of these shields were fabricated and annealed for JPL by the Williams Manufacturing Company, San Jose, California.

Fig. 1 is a cross-section of the fluxtank (magnetic shield) designed for thermal-vacuum testing of magnetometers. The tank consists of two coaxial cylindrical shells both with 0.060-in.-thick Mumetal walls. The inner and outer shells are held together with spot-welded Mumetal braces so that the two shields are a single physical unit. The design goals for this fluxtank were to achieve a reduction of the geomagnetic field (approximately 50,000 $\gamma$) to less than 360 $\gamma$ and to allow the evacuation of the interior volume. Numerous 0.5-in. holes were drilled in both shells to minimize impedance to evacuation. The drilling of holes is counter to good shielding design; however, the field in the sensor test volume is less than 30 $\gamma$ when Lid 1 is in place. This tank has been successfully used in the thermal-vacuum testing of both prototype and flight magnetometers and makes possible an evaluation of the instrument in its operating range during testing.

Fig. 2 is a cross-section of the fluxtank developed to support both bench testing of the *Mariner C* magnetometers and calibration verifications at the Air Force Eastern Test Range (AFETR). This tank also consists of inner and outer cylinders, but the inner shield is mechanically independent of the outer shield to minimize mechanical stresses. The design goals for this tank were maximum shielding against both the geomagnetic field

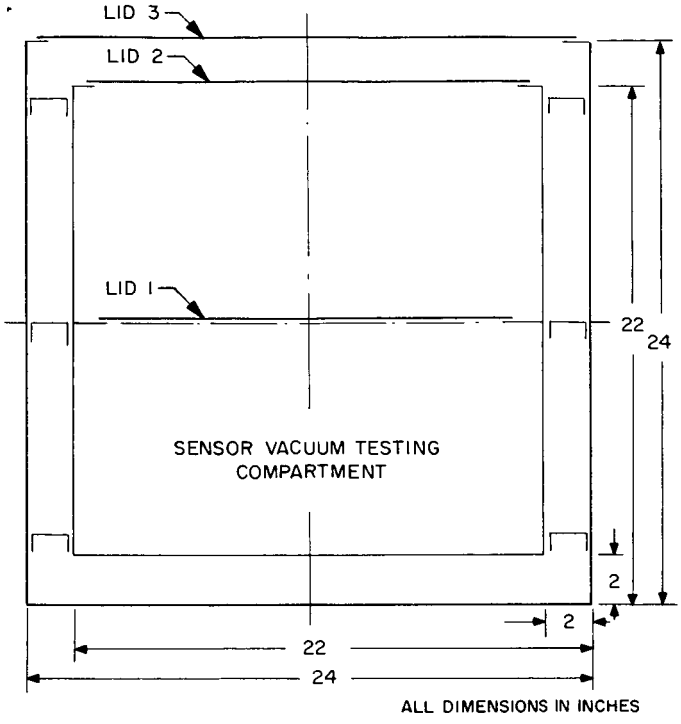


**Fig. 1. Magnetic shield for thermal-vacuum testing**

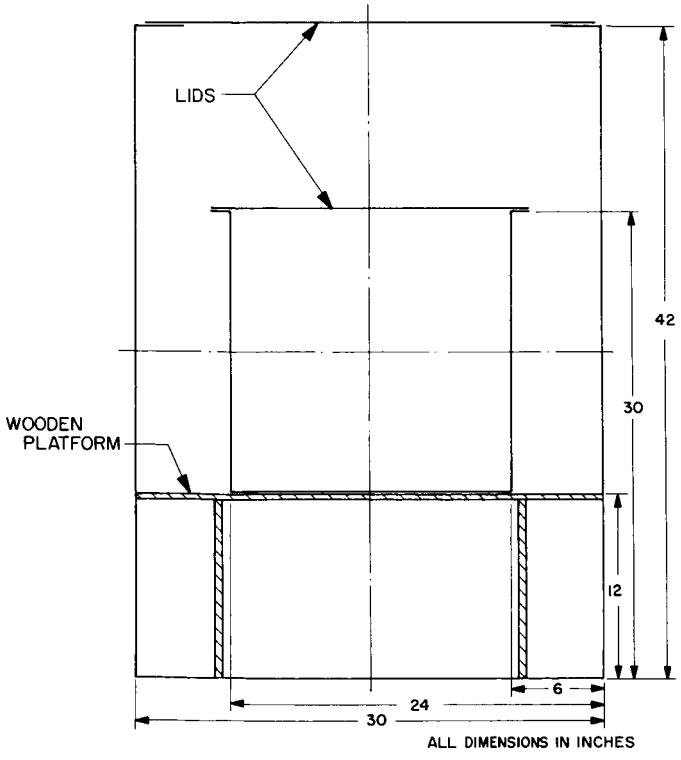


**Fig. 2. Magnetic shield for bench testing and calibration**

and laboratory magnetic disturbances, and long-term stability. The working volume is large enough to allow the magnetometer sensor to be rotated 180 deg in two perpendicular planes for making offset measurements. Tests conducted using a *Mariner C* helium magnetometer show that:

(1) The field in the shielded volume varies less than 0.1 $\gamma$ in 12 hr.

(2) The field in the test volume is 14 $\gamma$ (e.g., a shielding factor of 3600).

(3) The incremental shielding is approximately 2000 (a truck passing within 10 ft of the shield causes about a 0.1-$\gamma$ disturbance).

This tank was used for calibration verification of the *Mariner C-4* magnetometer at the AFETR. The calibration at the AFETR was in agreement with that obtained in the shielded room at the JPL magnetic facility at the Mesa Antenna Range.

The shielding factor equations for finite-length coaxial cylinders have not been derived, but, for design guidelines, the equations for concentric spherical shells[1] have been useful. The equation for a two-stage spherical shield can be written as

$$S = \frac{4}{9}\frac{t_1 t_2}{R_1 R_2}\mu_1\mu_2\left[1 - \left(\frac{R_1}{R_2}\right)^3\right]$$

where $S$ is the shielding factor; $R_1$ and $R_2$ are the radii of the inner and outer shells, respectively; $t_1$ and $t_2$ are the thicknesses of the inner and outer shells, respectively; and $\mu_1$ and $\mu_2$ are the permeabilities of the inner and outer shells, respectively.

The values of the permeability can be found from manufacturers' data[2]; the presence of any air gaps in the shield, however, appreciably reduce the effective permeability of a fabricated shell. The computed shielding factor for the tank shown in Fig. 2 is approximately 20,000 as compared to the measured value of 3600. To achieve a higher shielding factor than that achieved with this shield would require a fairly sophisticated lid closure device.

[1] Schweitzer, F., "Magnetic Shielding Factors of a System of Concentric Spherical Shells," *Journal of Applied Physics*, Vol. 33, pp. 1001–1003, March 1962.

[2] *Electrical Materials Handbook*, Allegheny Ludlum Steel Corporation, Pittsburgh, Pennsylvania, 1961.